Jordanian Journal of Computers and Information Technology (JJCIT), Vol. 12, No. 03, September 2026.

NETWORK PERFORMANCE OF TWO-WAY RELAYING WITH FOUNTAIN CODING IN WIRELESS SENSOR NETWORKS UNDER CO-CHANNEL INTERFERENCE

Duy-Hung Ha[1], Kien-Duc Tran[2], Dac-Binh Ha[3], Hien-Luong Nguyen[4], The-Anh Ngo[5] and Quoc-Hao Truong[6]

(Received: 22-May-2026, Revised: 4-Aug.-2026, Accepted: 20-Aug.-2026)

ABSTRACT

This paper investigates the performance of a two-way relay network (TWRN) for wireless sensor networks (WSNs) that combines fountain coding (FC) and digital network coding (DNC) in the presence of co- channel interference (CCI). A three-phase FC–DNC transmission protocol (SM-3P-FC) is considered and compared with the conventional four-phase fountain-coded protocol (SM-4P-FC). To isolate the contribution of fountain coding, an additional same-budget three-phase uncoded fixed-repetition benchmark (SM-3P-NoFC) is introduced, in which the Q transmission opportunities are distributed among H distinct uncoded packets. Under independent block-Rayleigh fading, closed-form analytical expressions for the outage probabilities at the two terminal nodes are derived by accounting for CCI at both the relay and the source nodes. Based on the derived outage probabilities, a bandwidth-normalized sum-throughput expression is further developed to characterize the trade-off between the target spectral efficiency and the probability of successful message recovery. Monte Carlo simulations based on 10^6 independently generated channel realizations per plotted point show close agreement with the derived analytical expressions over the evaluated parameter settings. The numerical results show that the proposed SM-3P-FC scheme achieves lower outage probabilities and higher bidirectional sum throughput than both the SM-3P-NoFC and SM-4P-FC benchmarks under the considered system settings. The additional CCI-power comparison further shows that the outage probabilities continue to decrease when interference is absent or when its power remains fixed, whereas proportional desired/interference power scaling produces non-zero outage floors.

KEYWORDS

Fountain coding, Digital network coding, Two-way relay network, Three-phase transmission, Co-channel interference, Outage probability, Sum throughput, Rayleigh fading.

1. INTRODUCTION

In dense or infrastructure-limited wireless sensor networks (WSNs), two sensor-cluster heads or aggregation nodes may need to exchange control or sensed-data packets through an intermediate relay, because the direct link is unavailable or insufficiently reliable. Such nodes typically operate under limited energy, transmit power, memory and processing capability. Therefore, reducing the number of transmission phases and limiting packet-specific retransmissions are important for transmission latency and energy efficiency in WSN deployments [24][39]. In the link-level abstraction adopted in this work, S_1 and S_2 may represent two sensor-cluster heads or aggregation nodes, whereas R represents an intermediate relay or gateway.

A two-way relay network (TWRN) is attractive in this setting, because it enables two end nodes to exchange information through a common relay while using fewer radio resources than two independent one-way relay transmissions [1]–[4]. However, frequency reuse among neighboring sensor clusters or communication devices may generate co-channel interference (CCI) at both the relay and the terminal nodes. This interference reduces the received signal-to-interference- plus-noise ratio

1. D.-H. Ha (Corresponding Author) is with Faculty of Information Technology, Ton Duc Thang University, Ho Chi Minh City, Vietnam. Email: haduyhung@tdtu.edu.vn
2. K.-D. Tran is with Faculty of Electrical and Electronics Engineering, Ton Duc Thang University, Ho Chi Minh City, Vietnam. Email: trankienduc.st@tdtu.edu.vn
3. D.-B. Ha is with School of Engineering and Technology, Duy Tan University, Da Nang, Vietnam. Email: hadacbinh@duytan.edu.vn
4. H.-L. Nguyen is with Department of Human Resources and Administration, Ton Duc Thang University, Ho Chi Minh City, Vietnam. Email: nguyenhienluong@tdtu.edu.vn
5. T.-A. Ngo is with Faculty of Engineering and Technology, Campus in Ho Chi Minh City, University of Transport and Communications, Hanoi, Vietnam. Email: anhnt_ph@utc.edu.vn
6. Q.-H. Truong is with Go Dau Infrastructure Center – VNPT. Email: truongquochao9792@gmail.com

and may cause packet-decoding failures, particularly in dense or power-limited WSN deployments [6]–[8].

Digital network coding (DNC) and fountain coding (FC) address different, but complementary, aspects of this problem. DNC allows the relay to combine two successfully decoded packets through a packet-level XOR operation and thereby complete the bidirectional exchange in three transmission phases instead of four. FC improves packet-level recovery by allowing a destination to reconstruct a source block after collecting a sufficient number of encoded packets, rather than requiring every particular encoded packet to be successfully delivered [3][20]. Consequently, the joint use of TWR, DNC and FC is motivated by the need to reduce the exchange duration while maintaining reliable packet recovery in the presence of CCI.

Accordingly, this work focuses on the packet-level outage probability and bandwidth-normalized bidirectional sum throughput of a terrestrial FC–DNC-assisted two-way relay link operating under CCI. The WSN context is represented through a physical- and link-layer abstraction of resource-constrained bidirectional packet exchange, while higher-layer routing, medium-access- control and network-management functions are beyond the scope of this study. This abstraction isolates the trade-off among transmission-phase reduction, fountain-code recovery and co-channel interference in a WSN-motivated two-way relay segment.

Existing studies related to the present work can be broadly classified into three research directions. The first research direction concerns interference-aware and multi-user two-way relaying. Nguyen and Do [6] analyzed a two-way NOMA network in which CCI affects both the relay and the destination nodes, while considering full-duplex and half-duplex operation together with successive interference cancellation. Nam et al. [7] investigated an interference-cancellation-aided cognitive two-way relay network with primary transmit-antenna selection/selection combining and secondary partial relay selection. Ozduran and Soleimani-Nasab [8] further studied multi-user two-way relaying in the presence of CCI and evaluated its impact on the achievable sum-rate performance.

For multi-user amplify-and-forward (AF) bidirectional relaying, opportunistic source-pair selection (OSPS) was introduced to mitigate inter-cell interference (ICI) by activating an appropriate source pair according to a sum-rate-based criterion [31]. This OSPS approach was subsequently analyzed in greater detail for multi-user two-way relay networks, where maximum-sum-capacity source-pair selection was shown to provide multi-user diversity and improved performance relative to simultaneous transmission and max–min selection [32]. Its robustness under imperfect channel state information (CSI) resulting from feedback delay and channel-estimation error (CEE) was further investigated in [33].

Related studies have also examined more advanced interference-aware two-way relay architectures. Ozduran et al. [34] analyzed power-domain NOMA for full-duplex two-way relaying and evaluated outage probability, error probability, ergodic rate and throughput while optimizing the transmit powers, power-allocation coefficients and relay position. Ozduran [35] investigated the secrecy achievable rate of an illegitimate full-duplex DF NOMA two-way relay network affected by CCI and friendly jamming. In addition, the impact of CCI on sum-rate-based opportunistic relay selection in dual-hop multiple full-duplex bidirectional relaying was studied in [36].

These studies demonstrate that source-pair scheduling, relay selection, NOMA, full-duplex operation and interference-management mechanisms can significantly improve the performance of bidirectional relay networks. However, their primary objectives are multi-user interference coordination, full-duplex NOMA, relay selection or physical-layer security. They do not jointly consider packet-level fountain coding and digital network coding, nor do they provide a matched SM-3P-FC/SM-4P-FC analysis with explicit CCI at the relay and both terminal nodes.

The second research direction employs fountain coding in cooperative and two-way relay networks. Fountain-coded cooperative schemes allow a destination to recover a source message after collecting a sufficient number of encoded packets, thereby improving reliability under packet loss and fading. Recent extensions have integrated fountain coding with cognitive-radio operation, reconfigurable intelligent surfaces and radio-frequency energy harvesting [20]. Nevertheless, these systems address different network architectures and do not provide a matched comparison between three-phase and four-phase transmission under explicit co-channel interference at all receiving nodes.

The third research direction focuses on fountain-coded and network-coded two-way relaying. Hau et al. investigated a secure multi-cast two-way relaying system employing fountain coding, three-phase digital network coding and randomize-and-forward transmission [26]. Their analysis considered outage probability, intercept probability, system-outage probability and system-intercept probability over Rayleigh-fading channels.

Toan et al. considered a secure two-way hybrid satellite–terrestrial relay system employing fountain coding, successive interference cancellation, digital network coding, partial relay selection and cooperative jamming [27]. In that scheme, the satellite and ground users simultaneously transmit encoded packets to the relay stations in the first phase, after which a selected relay performs an XOR operation and broadcasts the resulting packet in the second phase.

Recent studies published in 2024–2026 have further extended fountain coding to a variety of relay architectures. Nguyen et al. [20] investigated a fountain-coded two-way cognitive relaying network employing a reconfigurable intelligent surface and radio-frequency energy harvesting. Hau et al. [26] considered a secure multi-cast two-way relaying system combining fountain coding, three-phase digital network coding and randomize-and-forward transmission. Other recent studies employed fountain coding in hybrid satellite–terrestrial NOMA relay systems with RIS assistance or partial relay selection and physical-layer security [15].

More recently, Toan et al. [44] investigated fountain-coded hybrid satellite–terrestrial relay multi-cast under co-channel interference. They derived exact outage and system-outage probability expressions and formulated a joint time- and power-allocation problem to improve system reliability. Although that work explicitly considers both fountain coding and CCI, it focuses on one-way satellite-assisted multicast rather than terrestrial bidirectional relaying with DNC.

Among these works, the scheme in [26] is the closest to the present study, because it already combines two-way relaying, fountain coding and three-phase digital network coding. This confirms that these individual techniques have already been combined in related two-way relay architectures. Nevertheless, the existing studies focus on secure multicast, cognitive-radio, RIS-assisted, energy-harvesting or hybrid satellite–terrestrial systems. They do not provide a unified closed- form analysis of a terrestrial two-way relay network in which co-channel interference explicitly affects the relay and both terminal nodes. Moreover, they do not provide matched comparisons among SM-3P-FC, SM-4P-FC and a same-budget SM-3P-NoFC benchmark under identical channel, interference and power conditions.

From a WSN perspective, the unresolved issue is the absence of a unified evaluation of the three requirements that motivate the considered link-level scenario: reduced-phase bidirectional packet exchange, flexible source-block recovery and explicit CCI at every receiving node. Interference-aware two-way relaying studies generally omit packet-level fountain coding, whereas recent fountain-coded relay studies mainly focus on cognitive-radio, RIS-assisted, energy-harvesting, security or hybrid satellite–terrestrial architectures. Consequently, their results do not directly quantify the separate reliability and throughput contributions of fountain coding and three- phase transmission under matched terrestrial channel, interference, power and packet-budget conditions.

Accordingly, the novelty of the present work does not lie in introducing fountain coding, digital network coding or three-phase relaying individually. Rather, it lies in the unified closed- form performance analysis of a terrestrial SM-3P fountain-coded DNC two-way relay network with explicit co-channel interference at the relay and both terminal nodes. The developed framework derives the end-node outage probabilities and a bandwidth-normalized bidirectional sum-throughput expression and provides matched comparisons among the proposed SM-3P-FC scheme, the conventional SM-4P-FC scheme and a same-budget SM-3P-NoFC benchmark under identical channel, interference and power conditions, with the same source-block size and transmission budget. These comparisons separately identify the reliability and throughput contributions of fountain coding and three-phase transmission.

Objective and Contributions

Motivated by the above WSN link-level scenario, this paper develops and analyzes a terrestrial three-phase TWR scheme that jointly employs fountain coding and digital network coding under co-channel interference. The primary objective is to quantify the separate and combined effects of fountain-code-based recovery and three-phase transmission on the outage probability and bandwidth-normalized bidirectional sum throughput when the relay and both terminal nodes are exposed to CCI. The proposed SM-3P-FC scheme is analytically and numerically compared with both the conventional SM-4P-FC protocol and a same-budget three-phase uncoded fixed-repetition benchmark, denoted by SM-3P-NoFC. The main contributions of this work are summarized as follows:

- We develop an SM-3P-FC architecture that jointly incorporates fountain coding, packet-level digital network coding and co-channel interference in a two-way relay network. The considered model explicitly accounts for interference at the relay and both terminal nodes.
- We derive closed-form expressions for the per-round packet-delivery probabilities and the resulting outage probabilities at both terminal nodes over independent block-Rayleigh fading channels. The analysis explicitly captures the transmit powers, path-loss parameters, number of interferers, relay position, fountain-code recovery threshold H and maximum number of exchange rounds Q.
- Based on the derived outage probabilities, we develop a bandwidth-normalized bidirectional sum-throughput expression. This metric characterizes the trade-off among the target spectral efficiency, message-recovery probability and fountain-code parameters and reveals the existence of an optimum target-spectral efficiency for each transmission protocol.
- We conduct extensive Monte Carlo simulations to validate the analytical outage-probability and bidirectional sum-throughput expressions. The proposed SM-3P-FC scheme is evaluated against both the conventional SM-4P-FC protocol and a newly introduced same- budget SM-3P-NoFC benchmark. These comparisons separately reveal the performance contributions of fountain coding and the reduction in the number of transmission phases. The numerical results also quantify the effects of normalized transmit power, interference- power scaling, relay placement, H, Q and the number of co-channel interferers and provide engineering guidelines for interference-limited WSN and IoT deployments.

Table 1 summarizes the main differences between the present study and representative interference-aware, fountain-coded and network-coded two-way relaying works. The comparison shows that the individual components of the considered three-phase architecture have appeared in related contexts, whereas the present contribution focuses on their unified terrestrial CCI analysis and matched evaluations among the SM-3P-FC, SM-4P-FC and same-budget SM-3P-NoFC schemes.

Table 1. Comparison with representative related works.

Ref.	System and interference context	FC	Coding and transmission protocol	Metrics	Main distinction
Ref. [6]	Two-way NOMA with CCI at the relay and destination nodes	×	FD/HD relaying with perfect or imperfect SIC	OP	Analyzes the joint effects of CCI, duplex mode and SIC, without fountain coding or a matched SM-3P-FC/SM-4P-FC comparison.
Ref. [7]	Underlay cognitive two-way relay network with interference cancellation	×	DNC, primary TAS/SC and secondary partial relay selection	OP	Studies interference management and relay selection in cognitive two-way relaying, but does not employ fountain coding.
Ref. [20]	Cognitive two-way relaying with RIS and RF energy harvesting	✓	Three-phase DNC with conventional and early-stopping FC schemes	OP, SOP and average transmissions	Focuses on cognitive-radio interference constraints, RIS and energy harvesting rather than explicit CCI at every receiving node.
Ref. [26]	Secure multi-cast two-way relaying in the presence of a passive eavesdropper	✓	Three-phase FC–DNC with randomize-and-forward transmission	OP, IP, SOP, and SIP	Combines FC and three-phase DNC for secure multi-cast and physical-layer security, rather than terrestrial CCI explicitly affecting the relay and both terminal nodes.
Ref. [27]	Secure hybrid satellite–errestrial two-way relaying with an eavesdropper and cooperative jammer	✓	Two-phase FC–DNC with SIC, partial relay selection and cooperative jamming	OP, SOP, IP, and SIP	Analyzes the security–reliability trade-off in a hybrid satellite–terrestrial system, rather than conventional terrestrial CCI at the relay and both terminal nodes.
This paper	Terrestrial TWRN with explicit CCI at the relay and both terminals	✓	Three-phase FC–DNC; matched SM-4P-FC and same-budget SM-3P-NoFC benchmarks	OP and bidirectional sum throughput	Derives closed-form end-node OP and bandwidth-normalized bidirectional sum throughput; provides matched comparisons among SM-3P-FC, SM-4P-FC and a same-budget SM-3P-NoFC benchmark under identical channel, interference and power conditions.

Jordanian Journal of Computers and Information Technology (JJCIT), Vol. 12, No. 03, September 2026.

Abbreviations

Abbreviation	Definition	Abbreviation	Definition
TWR	Two-way relaying	RF	Radio frequency
TWRN	Two-way relay network	IP	Intercept probability
WSN	Wireless sensor network	SOP	System-outage probability
IoT	Internet of Things	SIP	System-intercept probability
SM-3P	Three-phase transmission protocol	TAS/SC	Transmit-antenna selection/selection combining
SM-4P	Four-phase transmission protocol	AF	Amplify-and-forward
FC	Fountain coding	DF	Decode-and-forward
DNC	Digital network coding	ICI	Intercell interference
CCI	Co-channel interference	OSPS	Opportunistic source-pair selection
OP	Outage probability	CSI	Channel state information
SINR	Signal-to-interference-plus-noise ratio	CEE	Channel-estimation error
CDF	Cumulative distribution function	MAC	Multiple-access channel
PDF	Probability density function	BC	Broadcast channel
MC	Monte Carlo	LDPC	Low-density parity-check
AWGN	Additive white Gaussian noise	OFDM	Orthogonal frequency-division multiplexing
NOMA	Non-orthogonal multiple access	NoFC	Without fountain coding
FD/HD	Full-duplex/half-duplex	SM-3P-NoFC	Three-phase DNC benchmark without fountain coding
SIC	Successive interference cancellation	SM-3P-FC	Three-phase FC–DNC transmission protocol
RIS	Reconfigurable intelligent surface	SM-4P-FC	Four-phase fountain-coded transmission protocol

Main Notations

Notation	Definition
S_1, S_2	Terminal/source nodes
R	Intermediate relay node
I_k	The k-th co-channel interferer
K	Number of co-channel interferers
m_1, m_2	Original source messages generated by S_1 and S_2, respectively
X_1, X_2	Packet-level payloads transmitted by S_1 and S_2, respectively, in a representative exchange round; fountain-coded for the FC schemes and uncoded for the NoFC benchmark
$X_3 = X_1 \oplus X_2$	Packet-level network-coded packet generated at R when both source packets are successfully decoded
$\mathcal{M}(\cdot)$	Modulation mapping from a packet-level payload to its transmitted symbol
$x_i = \mathcal{M}(X_i), i \in \{1,2,3\}$	Unit-energy modulated symbol associated with packet-level payload X_i
u_k	Unit-energy interference symbol transmitted by I_k
n_b	AWGN sample at receiving node $b \in \{R, S_1, S_2\}$
σ_0^2	AWGN power at each receiving node
P_S	Common transmit power of S_1, S_2 and R
P_I	Transmit power of each co-channel interferer
$\Psi_S = P_S/\sigma_0^2$	Normalized desired-node transmit power
$\Psi_I = P_I/\sigma_0^2$	Normalized co-channel-interference power
h_{ab}	Small-scale fading coefficient of link $a \to b$
$g_{ab} = \lvert h_{ab}\rvert^2$	Channel power gain of link $a \to b$
d_{ab}	Distance between nodes a and b
$\lambda_{ab} = d_{ab}^{\beta}$	Exponential rate parameter of the channel power gain on link $a \to b$
β	Path-loss exponent
C_{th}	Target spectral-efficiency threshold
$\rho_{\text{th}} = 2^{3C_{\text{th}}} - 1$	SINR threshold for the SM-3P protocol
$\xi_{\text{th}} = 2^{4C_{\text{th}}} - 1$	SINR threshold for the SM-4P protocol
ω_1, ω_2	Auxiliary parameters used in the SM-3P probability analysis
ϑ_1, ϑ_2	Auxiliary parameters used in the SM-4P probability analysis
H	Number of source packets and, under the ideal zero-overhead abstraction, the minimum recovery threshold
H_{eff}	Effective practical recovery threshold accounting for fountain-code overhead
Q	Maximum number of packet-exchange rounds
N_i	Number of fountain-coded packets successfully received by terminal S_i over Q exchange rounds
$\theta_{X_i}^{(p)}$	Per-round successful delivery probability of packet-level payload X_i under protocol p
$\text{OP}_{S_i}^{(p)}$	Outage probability at terminal S_i under protocol p
$\eta_S^{(p)}$	Bandwidth-normalized throughput at terminal S_i under protocol p
$\eta_{sum}^{(p)}$	Bidirectional bandwidth-normalized sum throughput under protocol p

p	Protocol index, $p \in \{\text{SM-3P, SM-4P}\}$
N_{MC}	Number of independently generated channel realizations for each plotted point
$\mathcal{CN}(\mu, \sigma^2)$	Circularly symmetric complex Gaussian distribution with mean μ and variance σ^2
$\mathrm{Exp}(\lambda)$	Exponential distribution with rate parameter λ
$L = \lfloor Q/H \rfloor$	Minimum number of repetitions assigned to each uncoded source packet
$r = Q - LH$	Number of uncoded source packets assigned one additional repetition

The remainder of this paper is organized as follows. Section 2 presents the system and channel models and derives the outage-probability and sum-throughput expressions for the SM-3P-FC, SM-4P-FC and SM-3P-NoFC schemes. Section 3 provides the analytical and Monte Carlo simulation results and discusses the corresponding engineering design implications. Finally, Section 4 concludes the paper and outlines future research directions.

2. System Model and Performance Analysis

2.1 Common System Model and Three-Phase DNC Protocol (SM-3P)

The network topology, node locations, transmit-power definitions, CCI model, channel distributions and block-fading assumptions introduced in this sub-section are common to the SM-3P-FC, SM-4P-FC and SM-3P-NoFC schemes. The schemes differ only in their packet-generation and recovery rules, relay-processing operations and transmission-phase schedules. Accordingly, the common system assumptions are stated once in this sub-section, whereas Sub-sections 2.3 and 2.5 subsequently present only the protocol-specific operations and performance expressions.

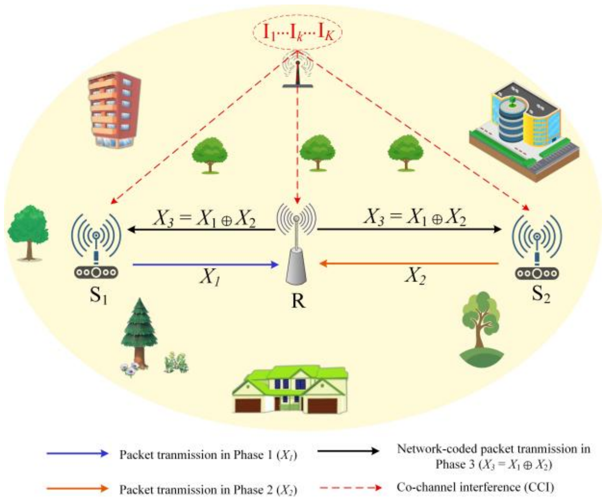

Figure 1. TWR model using DNC operating in a co-channel interference environment.

For clarity, Figure 1 illustrates the packet-level information flow of the three-phase protocol. The relay performs the XOR operation at the packet level as $X_3 = X_1 \oplus X_2$. Before transmission over the wireless channel, each packet-level payload X_i is mapped to the corresponding unit-energy modulated symbol $x_i = \mathrm{M}(X_i)$, $i \in \{1,2,3\}$, as used in the subsequent signal model.

The considered three-phase two-way relay network with DNC, hereafter denoted by SM-3P, consists of two source nodes, S_1 and S_2 and an intermediate relay R. Direct communication between S_1 and S_2 is unavailable (e.g., due to being out of range or obstructed), so both sources rely on R [25]. The network also includes K co-channel interferers affecting the network, denoted by $I_1, I_2, \ldots, I_K$. Such co-channel interference arises from frequency reuse, in which the spectrum is reused to improve spectral efficiency.

For the fountain-coded schemes, S_1 and S_2 generate fountain-coded packets and exchange them over successive packet-exchange rounds. Let X_1 and X_2 denote the packet-level payloads transmitted by S_1 and S_2, respectively, in a representative exchange round. Their corresponding unit-energy modulated symbols are denoted by $x_1 = M(X_1)$ and $x_2 = M(X_2)$. For notational simplicity, the exchange-round index is omitted from the instantaneous signal model.

Let m_1 and m_2 denote the original source messages generated by S_1 and S_2, respectively. To recover

m_2, terminal S_1 must successfully collect at least H fountain-coded packets generated by S_2. Similarly, S_2 must collect at least H fountain-coded packets generated by S_1 to recover m_1. The exchange proceeds for at most Q packet-exchange rounds, after which a terminal is considered to be in outage if it has collected fewer than H required encoded packets.

The present analysis adopts an ideal packet-level fountain-coding model. Specifically, H denotes the number of source packets and, under the adopted zero-overhead abstraction, also the minimum number of correctly received encoded packets assumed to be sufficient for successful source-message recovery, whereas Q denotes the maximum number of packet-exchange rounds.

In a practical fountain-code implementation, successful decoding may require more than H correctly received encoded packets because of finite-length and degree-distribution overhead. At the present packet-level abstraction, this overhead may be approximated by replacing H with an effective recovery threshold $H_{eff} > H$. The excess H_{eff} - H depends on the selected code construction, degree distribution, source-block length and decoding algorithm. The degree distribution also affects the sparsity of the decoding graph and therefore the number of decoding operations, memory usage, processing latency and energy consumption at resource-constrained WSN nodes [28]-[29].

This effective-threshold substitution is only a packet-level approximation of finite-length fountain decoding. A code-specific analysis would additionally require a decoding-success function that depends on the number of correctly received packets, source-block length, degree distribution, code construction and decoding algorithm. Under the effective-threshold approximation, the predicted outage probability generally increases and the effective throughput decreases.

If R successfully decodes only packet X_1, but not packet X_2, it forwards X_1 to S_2 in the third time slot by transmitting the corresponding modulated symbol x_1=$M(X_1)$. Conversely, if R successfully decodes X_2, but not X_1, it forwards X_2 to S_1 by transmitting x_2 =$M(X_2)$.

Under the DNC method, the exchange over three time slots operates as follows. In the first two time slots, S_1 and S_2 transmit $x_1 = M(X_1)$ and $x_2 = M(X_2)$ to R, respectively; the transmission order is immaterial and does not affect performance. The relay then attempts to decode the packet-level payloads X_1 and X_2. If both packets are successfully decoded, R forms the packet-level network-coded packet, maps it to the unit-energy modulated symbol $x_3 = M(X_3)$ and broadcasts x_3 to S_1 and S_2 in the third time slot.

$$X_3 = X_1 \oplus X_2,$$

Protocol-specific differences: Within the unified system model, the SM-3P-FC and SM-3P-NoFC schemes employ the same three-phase physical transmission schedule and the same packet-level DNC operation. In the first phase, S_1 transmits $x_1 = M(X_1)$ to R and in the second phase, S_2 transmits $x_2 = M(X_2)$ to R. In the third phase, if both packets X_1 and X_2 are successfully decoded, the relay forms $X_3 = X_1 \oplus X_2$ and broadcasts $x_3 = M(X_3)$ to both terminal nodes. If only one packet is successfully decoded, the relay forwards that packet to its intended destination. If neither packet is decoded, the relay remains silent during the third phase.

Table 2. Transmission-phase schedules of the considered schemes.

Scheme	Phase 1	Phase 2	Relay phase(s)
SM-3P-FC	$S_1 \to R$	$S_2 \to R$	Phase 3: $R \to \{S_1, S_2\}$ using $X_3 = X_1 \oplus X_2$
SM-3P-NoFC	$S_1 \to R$	$S_2 \to R$	Phase 3: $R \to \{S_1, S_2\}$ using $X_3 = X_1 \oplus X_2$
SM-4P-FC	$S_1 \to R$	$S_2 \to R$	Phase 3: $R \to S_2$; Phase 4: $R \to S_1$

The difference between SM-3P-FC and SM-3P-NoFC lies in the packet-generation and source-message-recovery rules rather than in the physical transmission schedule. In SM-3P-FC, each source generates fountain-coded packets and the destination can recover the source message after collecting any H successfully received encoded packets over at most Q exchange rounds.

In SM-3P-NoFC, each source instead transmits H distinct uncoded packets according to a fixed repetition schedule and successful recovery requires every distinct source packet to be received at least once. By contrast, SM-4P-FC uses the same network topology, transmit-power definitions, CCI model and channel assumptions, but it forwards the two communication directions separately over four phases:

$S_1 \longrightarrow R$, $R \longrightarrow S_2$, $S_2 \longrightarrow R$ and $R \longrightarrow S_1$. Therefore, SM-4P-FC does not employ the packet-level XOR broadcast used by the two SM-3P schemes. The transmission-phase schedules of the three considered schemes are summarized in Table 2.

Practical implementation considerations: In an actual implementation, each destination must identify and buffer the successfully received encoded packets and then execute the selected fountain-decoding algorithm. The packet headers or coding metadata must also provide sufficient information for the decoder to determine the relationships among the received encoded packets. At the relay, the received signals from the two sources must be demodulated and decoded at the packet level. The successfully recovered encoded packets are then stored when necessary, combined through packet-level XOR when both packets are available, remodulated and broadcast to the terminal nodes.

These operations introduce packet-header overhead, signaling, buffering, memory usage, processing delay, decoding complexity and energy consumption. Such implementation costs can be significant for resource-constrained WSN devices. They are not included in the present outage analysis, the purpose of which is to isolate the effects of fading, co-channel interference, fountain-code recovery parameters and the number of transmission phases.

Transmission-phase and reciprocity assumptions: Unlike the two-phase MAC/BC information exchange considered in Ref. [8], the adopted SM-3P protocol employs two orthogonal source-to-relay time slots followed by one relay broadcast time slot. Specifically, S_1 transmits to Rin the first time slot, S_2 transmits to Rin the second time slot and R broadcasts or forwards the recovered packet information in the third time slot. Therefore, the first two time slots do not constitute a simultaneous two-user MAC phase.

The forward and reverse links between S_i and R, $i \in \{1,2\}$, have the same propagation distance and hence share the same large-scale channel parameter, i.e., $\lambda_{S_iR} = \lambda_{RS_i} = d_{S_iR}^{\beta}$.

For notational simplicity, $\lambda_{S_iR}$is used for both directions. However, the transmissions $Si \longrightarrow R$ and $R \longrightarrow S_i$ occur in different time slots and their small-scale fading coefficients are modeled as independent realizations. Consequently, instantaneous channel reciprocity is not assumed, although the forward and reverse links have the same marginal distribution.

Signal-normalization and channel assumptions: The modulated symbols $x_i = \mathcal{M}(X_i)$, $i \in \{1,2,3\}$ and the interference symbols u_k are assumed to have unit average energy, i.e., $\mathbb{E}\left[\left|x_j\right|^2\right] = 1, j \in \{1,2,3\}$, and $\mathbb{E}[|u_k|^2] = 1, k \in \{1, \dots, K\}$.

The interference symbols are mutually independent and are independent of the desired transmitted symbols, channel coefficients and receiver noise. The AWGN sample at receiving node $b \in \{R, S_1, S_2\}$ is modeled as: $n_b \sim \mathcal{CN}(0, \sigma_0^2)$.

All desired and interfering links experience independent block-Rayleigh fading [37]. More specifically, $h_{S_iR} \sim \mathcal{CN}\left(0, \lambda_{S_iR}^{-1}\right), h_{RS_i} \sim \mathcal{CN}\left(0, \lambda_{S_iR}^{-1}\right), i \in \{1,2\}$, whereas $h_{I_kb} \sim \mathcal{CN}\left(0, \lambda_{I_kb}^{-1}\right), k \in \{1, \dots, K\}, b \in \{R, S_1, S_2\}$.

Accordingly, each channel power gain satisfies $g_{ab} = |h_{ab}|^2 \sim \mathrm{Exp}(\lambda_{ab})$.

Each channel coefficient remains constant within one time slot and is independently regenerated across different time slots and packet-exchange rounds. The fading coefficients of distinct desired and interfering links are mutually independent. The node locations, transmit powers and link-specific marginal channel distributions remain unchanged over the Q exchange rounds.

2.1.1 First Time Slot

The signal received at R when S_1 transmits the unit-energy modulated symbol $x_1 = \mathcal{M}(X_1)$ associated with packet X_1 in the presence of the co-channel interferers is given by [7]:

$$y_{S_1 \to R} = \sqrt{P_S} h_{S_1R} x_1 + \sum_{k=1}^{K} \sqrt{P_I} h_{I_kR} u_k + n_R, \tag{1}$$

where P_S denotes the common transmit power used by S_1, S_2 and R, whereas P_I denotes the common transmit power of each co-channel interferer. This equal-power assumption is applied within each transmitter group to simplify the analysis; no equality between P_S and P_I is imposed in the analytical derivations. The coefficients h_{S_1R} and h_{I_kR} denote the Rayleigh fading coefficients of the $S_1 \to R$ and $I_k \to R$ links, respectively, where $k \in \{1,2,\dots,K\}$.

From Eq. (1), the instantaneous signal-to-interference-plus-noise ratio (SINR) at R in the first time slot is expressed as:

$$\varphi_{S_1R} = \frac{P_S\left|h_{S_1R}\right|^2}{\sum_{k=1}^{K} P_I\left|h_{I_kR}\right|^2 + \sigma_0^2} = \frac{\Psi_S g_{S_1R}}{\sum_{k=1}^{K} \Psi_I g_{I_kR} + 1}, \tag{2}$$

where $g_{S_1R} = \left|h_{S_1R}\right|^2, g_{I_kR} = \left|h_{I_kR}\right|^2, \Psi_S = P_S/\sigma_0^2$ and $\Psi_I = P_I/\sigma_0^2$.

For subsequent averaging over the desired and interfering channel gains, the marginal CDFs and PDFs of g_{S_1R} and g_{I_kR} are given by:

$$\begin{aligned} F_{g_{S_1R}}(x) &= 1 - \exp\left(-\lambda_{S_1R}x\right), F_{g_{I_kR}}(x) = 1 - \exp\left(-\lambda_{I_kR}x\right), \\ f_{g_{S_1R}}(x) &= \lambda_{S_1R}\exp\left(-\lambda_{S_1R}x\right), f_{g_{I_kR}}(x) = \lambda_{I_kR}\exp\left(-\lambda_{I_kR}x\right). \end{aligned} \tag{3}$$

where $\lambda_{S_1R} = \left(d_{S_1R}\right)^\beta$ and $\lambda_{I_kR} = \left(d_{I_kR}\right)^\beta$. Here, d_{S_1R} and d_{I_kR} denote the corresponding link distances and β is the path-loss exponent, which typically satisfies $2 \le \beta \le 6$, depending on the propagation environment [38]. It should be emphasized that Eq. (3) characterizes the marginal distributions of the individual desired and interfering channel power gains; it is not the CDF of the SINR in Eq. (2). The aggregate CCI term in Eq. (2), $\sum_{k=1}^{K} \Psi_I g_{I_kR}$, is explicitly retained in the SINR expression and is subsequently accounted for by averaging over the joint distribution of the K independent interference gains, as shown in Eqs. (21-23). Accordingly, the instantaneous channel capacity at R (in this slot) is:

$$C_{S_1R} = \frac{1}{3}\log_2\left(1 + \varphi_{S_1R}\right) = \frac{1}{3}\log_2\left(1 + \frac{\Psi_S g_{S_1R}}{\sum_{k=1}^{K} \Psi_I g_{I_kR} + 1}\right). \tag{4}$$

Note: For a fair comparison between the three-phase TWR model (DNC) and the conventional four-phase TWR model, assume that the total transmission time per packet exchange is the same (normalized to one time unit) in both models. Since the SM-3P uses three time slots, each slot occupies one third of that time; this explains the factor $\frac{1}{3}$ preceding the logarithm in Eq. (4).

2.1.2 Second Time Slot

Similarly, when S_2 transmits the unit-energy modulated symbol $x_2 = \mathcal{M}(X_2)$ associated with packet X_2, the signal received at R is given by [7]:

$$y_{S_2\to R} = \sqrt{P_S}h_{S_2R}x_2 + \sum_{k=1}^{K} \sqrt{P_I}h_{I_kR}u_k + n_R, \tag{5}$$

where h_{S_2R} denotes the channel coefficient of the $S_2 \to R$ link.

Hence, the instantaneous SINR at R in the second time slot is expressed as:

$$\varphi_{S_2R} = \frac{P_S\left|h_{S_2R}\right|^2}{\sum_{k=1}^{K} P_I\left|h_{I_kR}\right|^2 + \sigma_0^2} = \frac{\Psi_S g_{S_2R}}{\sum_{k=1}^{K} \Psi_I g_{I_kR} + 1}, \tag{6}$$

where $g_{S_2R} = \left|h_{S_2R}\right|^2$.

The CDF and PDF of g_{S_2R} are respectively given by:

$$F_{g_{S_2R}}(x) = 1 - \exp\left(-\lambda_{S_2R}x\right), f_{g_{S_2R}}(x) = \lambda_{S_2R}\exp\left(-\lambda_{S_2R}x\right), \tag{7}$$

where $\lambda_{S_2R} = \left(d_{S_2R}\right)^\beta$, with d_{S_2R} denoting the distance between S_2 and R.

Similarly, Eq. (7) gives the marginal distribution of the desired channel power gain g_{S_2R}, rather than the CDF of the SINR in Eq. (6). The aggregate CCI term in Eq. (6) remains explicitly included and is treated through the same probability-averaging procedure used for the first source-to-relay link.

Using the instantaneous SINR in Eq. 6, the channel capacity of the $S_2 \to R$ link in the second time slot is given by:

$$C_{S_2R} = \frac{1}{3}\log_2\left(1+\varphi_{S_2R}\right) = \frac{1}{3}\log_2\left(1+\frac{\Psi_S g_{S_2R}}{\sum_{k=1}^{K} \Psi_I g_{I_kR}+1}\right). \quad (8)$$

Note: The relay R successfully decodes packet X_1 if $C_{S_1R} \geq C_{\text{th}}$ and it successfully decodes packet X_2 if $C_{S_2R} \geq C_{\text{th}}$. Otherwise, the corresponding packet-decoding operation is considered unsuccessful; i.e., when the corresponding instantaneous capacity is below C_{th}.

2.1.3 Third Time Slot

Therefore, four cases arise when R attempts to decode the packet-level payloads X_1 and X_2:

- Case 1: R successfully decodes both X_1 and X_2
$$C_{S_1R} \geq C_{\text{th}} \text{ and } C_{S_2R} \geq C_{\text{th}}.$$
- Case 2: R successfully decodes X_1, but fails to decode X_2
$$C_{S_1R} \geq C_{\text{th}} \text{ and } C_{S_2R} < C_{\text{th}}.$$
- Case 3: R successfully decodes X_2, but fails to decode X_1
$$C_{S_1R} < C_{\text{th}} \text{ and } C_{S_2R} \geq C_{\text{th}}.$$
- Case 4: R fails to decode both X_1 and X_2
$$C_{S_1R} < C_{\text{th}} \text{ and } C_{S_2R} < C_{\text{th}}.$$

a) Case 1: $C_{S_1R} \geq C_{\text{th}}$ and $C_{S_2R} \geq C_{\text{th}}$.

In this case, R successfully decodes both packet-level payloads X_1 and X_2, forms $X_3 = X_1 \oplus X_2$ and broadcasts the corresponding modulated symbol $x_3 = \mathcal{M}(X_3)$. The received signals at S_1 and S_2 are respectively expressed as:

$$y_{R\to S_1} = \sqrt{P_S} h_{RS_1} x_3 + \sum_{k=1}^{K} \sqrt{P_I} h_{I_kS_1} u_k + n_{S_1},$$
$$y_{R\to S_2} = \sqrt{P_S} h_{RS_2} x_3 + \sum_{k=1}^{K} \sqrt{P_I} h_{I_kS_2} u_k + n_{S_2}, \quad (9)$$

where h_{RS_1} and h_{RS_2} denote the channel coefficients of the $R \to S_1$ and $R \to S_2$ links, respectively.

The summation term in each received signal represents the aggregate CCI observed at the corresponding terminal. Therefore, the interference contributions are explicitly retained in the denominators of the instantaneous SINRs in Eqs. (10 and 11).

From the received signals in Eq. (9), the instantaneous SINRs at S_1 and S_2 are respectively obtained as:

$$\varphi_{RS_1} = \frac{P_S\left|h_{RS_1}\right|^2}{\sum_{k=1}^{K} P_I\left|h_{I_kS_1}\right|^2+\sigma_0^2} = \frac{\Psi_S g_{RS_1}}{\sum_{k=1}^{K} \Psi_I g_{I_kS_1}+1}, \quad (10)$$

$$\varphi_{RS_2} = \frac{P_S\left|h_{RS_2}\right|^2}{\sum_{k=1}^{K} P_I\left|h_{I_kS_2}\right|^2+\sigma_0^2} = \frac{\Psi_S g_{RS_2}}{\sum_{k=1}^{K} \Psi_I g_{I_kS_2}+1}, \quad (11)$$

where $g_{RS_1} = \left|h_{RS_1}\right|^2$, $g_{RS_2} = \left|h_{RS_2}\right|^2$, $g_{I_kS_1} = \left|h_{I_kS_1}\right|^2$ and $g_{I_kS_2} = \left|h_{I_kS_2}\right|^2$.

Note: Consistent with the reciprocity assumptions stated above, g_{S_iR} and g_{RS_i} are independent small-scale fading realizations, because they correspond to different time slots, but they share the same exponential rate parameter $\lambda_{S_iR}, i \in \{1,2\}$.

Under the exponential channel-power model stated above, the marginal CDFs and PDFs of $g_{I_kS_1}$ and $g_{I_kS_2}$ are given by:

$$\begin{aligned} F_{g_{I_kS_1}}(x) &= 1-\exp\left(-\lambda_{I_kS_1}x\right), F_{g_{I_kS_2}}(x) = 1-\exp\left(-\lambda_{I_kS_2}x\right), \\ f_{g_{I_kS_1}}(x) &= \lambda_{I_kS_1}\exp\left(-\lambda_{I_kS_1}x\right), f_{g_{I_kS_2}}(x) = \lambda_{I_kS_2}\exp\left(-\lambda_{I_kS_2}x\right), \end{aligned} \quad (12)$$

where $\lambda_{I_k S_1} = \left(d_{I_k S_1}\right)^{\beta}$ and $\lambda_{I_k S_2} = \left(d_{I_k S_2}\right)^{\beta}$, with $d_{I_k S_1}$ and $d_{I_k S_2}$ denoting the distances from interferer I_k to the source nodes.

Eq. (12) gives the marginal distributions of the individual interference-channel power gains. It does not represent the distribution of the aggregate CCI or of the terminal SINRs. The aggregate interference powers are explicitly included in Eqs. (10 and 11), respectively and are subsequently incorporated into the packet-delivery probability analysis by averaging over the K independent interference gains.

$$\sum_{k=1}^{K} \Psi_I g_{I_k S_1} \text{ and } \sum_{k=1}^{K} \Psi_I g_{I_k S_2},$$

The channel capacity for the links is calculated using the following formulas:

$$C_{RS_1} = \frac{1}{3}\log_2\left(1 + \varphi_{RS_1}\right) = \frac{1}{3}\log_2\left(1 + \frac{\Psi_S g_{RS_1}}{\sum_{k=1}^{K} \Psi_I g_{I_k S_1} + 1}\right),$$

$$C_{RS_2} = \frac{1}{3}\log_2\left(1 + \varphi_{RS_2}\right) = \frac{1}{3}\log_2\left(1 + \frac{\Psi_S g_{RS_2}}{\sum_{k=1}^{K} \Psi_I g_{I_k S_2} + 1}\right) \tag{13}$$

Note: If $C_{RS_1} \geq C_{\text{th}}$, then S_1 successfully decodes packet X_3 from the received modulated symbol $x_3 = \mathcal{M}(X_3)$; otherwise, the decoding operation fails. Similarly, S_2 successfully decodes packet X_3 if $C_{RS_2} \geq C_{\text{th}}$. After decoding packet X_3, terminal S_1 recovers $X_2 = X_3 \oplus X_1$, whereas S_2 recovers $X_1 = X_3 \oplus X_2$. Each terminal then stores the recovered fountain-coded packet for subsequent source-message decoding.

b) Case 2: $C_{S_1 R} \geq C_{\text{th}}$ and $C_{S_2 R} < C_{\text{th}}$.

In this case, R successfully decodes packet X_1, but fails to decode packet X_2. Therefore, it forwards X_1 to S_2 by transmitting the corresponding symbol $x_1 = \mathcal{M}(X_1)$ in the third time slot. The received signal at S_2, together with its SINR and channel capacity, is given as follows [7]:

$$y_{R\to S_2} = \sqrt{P_S} h_{RS_2} x_1 + \sum_{k=1}^{K} \sqrt{P_I} h_{I_k S_2} u_k + n_{S_2}, \tag{14}$$

$$\varphi_{RS_2} = \frac{\Psi_S g_{RS_2}}{\sum_{k=1}^{K} \Psi_I g_{I_k S_2} + 1}, \tag{15}$$

$$C_{RS_2} = \frac{1}{3}\log_2\left(1 + \varphi_{RS_2}\right) = \frac{1}{3}\log_2\left(1 + \frac{\Psi_S g_{RS_2}}{\sum_{k=1}^{K} \Psi_I g_{I_k S_2} + 1}\right). \tag{16}$$

c) Case 3: $C_{S_1 R} < C_{\text{th}}$ and $C_{S_2 R} \geq C_{\text{th}}$ **.**

In this case, R successfully decodes packet X_2, but fails to decode packet X_1. Therefore, it forwards X_2 to S_1 by transmitting the corresponding symbol $x_2 = \mathcal{M}(X_2)$ in the third time slot. The received signal at S_1, together with its SINR and channel capacity, is given as follows [7]:

$$y_{R\to S_1} = \sqrt{P_S} h_{RS_1} x_2 + \sum_{k=1}^{K} \sqrt{P_I} h_{I_k S_1} u_k + n_{S_1}, \tag{17}$$

$$\varphi_{RS_1} = \frac{\Psi_S g_{RS_1}}{\sum_{k=1}^{K} \Psi_I g_{I_k S_1} + 1}. \tag{18}$$

$$C_{RS_1} = \frac{1}{3}\log_2\left(1 + \varphi_{RS_1}\right) = \frac{1}{3}\log_2\left(1 + \frac{\Psi_S g_{RS_1}}{\sum_{k=1}^{K} \Psi_I g_{I_k S_1} + 1}\right). \tag{19}$$

d) Case 4: $C_{S_1 R} < C_{\text{th}}$ and $C_{S_2 R} < C_{\text{th}}$.

In this case, if R fails to decode both X_1 and X_2, no data is transmitted in the third time slot. Consequently, both source nodes will not receive any new information during this phase, increasing the likelihood of an outage.

2.2 Probability Analysis Using the SM-3P Model

Because the total duration of one SM-3P packet-exchange round is normalized to one time unit and consists of three equal-duration transmission phases, the successful-decoding condition for an instantaneous SINR γ is transformed as:

$$\frac{1}{3}\log_2(1+\gamma) \geq C_{\text{th}} \Leftrightarrow \log_2(1+\gamma) \geq 3C_{\text{th}} \Leftrightarrow \gamma \geq 2^{3C_{\text{th}}} - 1 \triangleq \rho_{\text{th}}.$$

Thus, the factor three associated with the SM-3P transmission duration is absorbed into the SINR threshold ρ_{th} and is used throughout the following outage-probability derivation.

Because all channel power gains are continuously distributed, the probability of the boundary event $C = C_{\text{th}}$ is zero. Therefore, replacing the strict inequality by the non-strict inequality does not alter the derived outage probabilities. Nevertheless, the successful-decoding condition is consistently written using $\geq C_{\text{th}}$, whereas decoding failure is defined using $< C_{\text{th}}$. First, we derive the probability that packet X_1 is successfully delivered from S_1 to S_2. For S_2 to successfully receive packet X_1, both the $S_1 \to R$ and $R \to S_2$ transmissions must be successful. Since these transmissions occur in different time slots and their corresponding fading realizations are modeled as independent, the end-to-end success probability can be factorized as follows:

$$\theta_{X_1}^{\text{SM-3P}} = \Pr\left(C_{S_1R} \geq C_{\text{th}}\right)\Pr\left(C_{RS_2} \geq C_{\text{th}}\right)$$

$$= \Pr\left(\frac{1}{3}\log_2\left(1+\frac{\Psi_S g_{S_1R}}{\sum_{k=1}^{K}\Psi_I g_{I_kR}+1}\right) \geq C_{\text{th}}\right)\Pr\left(\frac{1}{3}\log_2\left(1+\frac{\Psi_S g_{RS_2}}{\sum_{k=1}^{K}\Psi_I g_{I_kS_2}+1}\right) \geq C_{\text{th}}\right)$$

$$= \Pr\left(\frac{\Psi_S g_{S_1R}}{\sum_{k=1}^{K}\Psi_I g_{I_kR}+1} \geq \rho_{\text{th}}\right)\Pr\left(\frac{\Psi_S g_{RS_2}}{\sum_{k=1}^{K}\Psi_I g_{I_kS_2}+1} \geq \rho_{\text{th}}\right), \quad (20)$$

Next, we calculate the probability term in Eq. (20) as follows:

$$\Pr\left(\frac{\Psi_S g_{S_1R}}{\sum_{k=1}^{K}\Psi_I g_{I_kR}+1} \geq \rho_{\text{th}}\right) = \Pr\left(\Psi_S g_{S_1R} \geq \rho_{\text{th}}\Psi_I\sum_{k=1}^{K} g_{I_kR}+\rho_{\text{th}}\right) \quad (21)$$

$$= \Pr\left(g_{S_1R \geq \omega_1}\sum_{k=1}^{K} g_{I_kR}+\omega_2\right), \quad (21)$$

with

$$\omega_1 = \frac{\rho_{\text{th}}\Psi_I}{\Psi_S}, \omega_2 = \frac{\rho_{\text{th}}}{\Psi_S}.$$

It is worth emphasizing that the above analytical expressions do not require equal desired-signal and interference powers. The unequal-power case is directly captured through $\Psi_S = P_S/\sigma_0^2$ and $\Psi_I = P_I/\sigma_0^2$. In particular, the outage behavior is governed by both the desired-node SNR Ψ_S and the power ratio Ψ_I/Ψ_S.

When P_S and P_I increase proportionally, Ψ_I/Ψ_S remains constant. Consequently, ω_1 remains non-zero while ω_2 approaches zero and the system converges to an interference-limited outage floor. In contrast, when P_S increases while P_I remains fixed, both ω_1 and ω_2 approach zero. Therefore, the outage probability continues to decrease and does not approach the same interference-limited floor. Conversely, increasing P_I for a fixed P_S increases ω_1 and degrades the packet- and message-recovery probabilities.

These observations indicate that separate power allocation for the desired nodes and interference management for the co-channel interferers can significantly affect system performance. Increasing the transmit power of the sources and relay is effective when the aggregate interference power remains bounded. However, proportional power scaling at all transmitting nodes cannot eliminate the outage floor. Hence, desired-node power allocation should be combined with interference-aware scheduling, resource allocation, interference cancellation, admission control or constraints on the admissible interference power. When the interferers are uncoordinated, the system may instead adapt P_S according to the measured interference level. Such mechanisms are particularly relevant to energyconstrained WSN deployments, where increasing P_S without considering the associated energy cost may not be practical. To evaluate the probability term in Eq. (21), we condition on the K independent interference-channel power gains by setting $g_{I_k R} = z_k, k = 1, \dots, K$.

Since one integration variable is associated with each co-channel interferer, averaging over their joint distribution requires a K-fold integral. Moreover, owing to the independence assumption, their joint PDF factorizes as: $f_{g_{I_1 R},\dots,g_{I_K R}}(z_1, \dots, z_K) = \prod_{k=1}^{K} f_{g_{I_k R}}(z_k)$.

Accordingly, the probability term is evaluated as:

$$\Pr\left(g_{S_1 R} \geq \omega_1 \sum_{k=1}^{K} g_{I_k R} + \omega_2\right) = \underbrace{\int_0^\infty \cdots \int_0^\infty}_{K-\text{fold integral}} \left[1 - F_{g_{S_1 R}}\left(\omega_1 \sum_{k=1}^{K} z_k + \omega_2\right)\right] \prod_{k=1}^{K} f_{g_{I_k R}}(z_k) dz_1 \cdots dz_K$$
$$= \exp(-\lambda_{S_1 R}\omega_2) \prod_{k=1}^{K} \int_0^\infty \lambda_{I_k R} \exp[-(\lambda_{I_k R} + \lambda_{S_1 R}\omega_1) z_k] dz_k = \exp(-\lambda_{S_1 R}\omega_2) \prod_{k=1}^{K} \frac{\lambda_{I_k R}}{\lambda_{I_k R} + \lambda_{S_1 R}\omega_1} \quad (22)$$

Using the same conditioning and K-fold averaging procedure, the success probability of the $R \rightarrow S_2$ link is obtained analogously. Multiplying the two independent link-success probabilities yields the per-round delivery probability of packet X_1 under the SM-3P protocol as:

$$\theta_{X_1}^{\text{SM-3P}} = \Pr(C_{S_1 R} \geq C_{\text{th}}) \Pr(C_{R S_2} \geq C_{\text{th}})$$
$$= \exp(-(\lambda_{S_1 R} + \lambda_{S_2 R})\omega_2) \prod_{k=1}^{K} \frac{\lambda_{I_k R}\lambda_{I_k S_2}}{(\lambda_{I_k R} + \lambda_{S_1 R}\omega_1)(\lambda_{I_k S_2} + \lambda_{S_2 R}\omega_1)} \quad (23)$$

Therefore, the per-round delivery-failure probability of packet X_1 at S_2 is given by:

$$1 - \theta_{X_1}^{\text{SM-3P}} = 1 - \exp(-(\lambda_{S_1 R} + \lambda_{S_2 R})\omega_2) \prod_{k=1}^{K} \frac{\lambda_{I_k R}\lambda_{I_k S_2}}{(\lambda_{I_k R} + \lambda_{S_1 R}\omega_1)(\lambda_{I_k S_2} + \lambda_{S_2 R}\omega_1)}. \quad (24)$$

Similarly, the per-round probability that S_1 successfully receives packet X_2 is given by:

$$\theta_{X_2}^{\text{SM-3P}} = \Pr(C_{S_2 R} \geq C_{\text{th}}) \Pr(C_{R S_1} \geq C_{\text{th}})$$
$$= \Pr\left(\frac{\Psi_S g_{S_2 R}}{\sum_{k=1}^{K} \Psi_I g_{I_k R} + 1} \geq \rho_{\text{th}}\right) \Pr\left(\frac{\Psi_S g_{R S_1}}{\sum_{k=1}^{K} \Psi_I g_{I_k S_1} + 1} \geq \rho_{\text{th}}\right)$$
$$= \exp(-(\lambda_{S_1 R} + \lambda_{S_2 R})\omega_2) \prod_{k=1}^{K} \frac{\lambda_{I_k R}\lambda_{I_k S_1}}{(\lambda_{I_k R} + \lambda_{S_2 R}\omega_1)(\lambda_{I_k S_1} + \lambda_{S_1 R}\omega_1)}. \quad (25)$$

The corresponding per-round delivery-failure probability of packet X_2 at S_1 is given by:

$$1 - \theta_{X_2}^{\text{SM-3P}} = 1 - \exp(-(\lambda_{S_1 R} + \lambda_{S_2 R})\omega_2) \prod_{k=1}^{K} \frac{\lambda_{I_k R}\lambda_{I_k S_1}}{(\lambda_{I_k R} + \lambda_{S_2 R}\omega_1)(\lambda_{I_k S_1} + \lambda_{S_1 R}\omega_1)}. \quad (26)$$

Now, we consider the outage probabilities at S_1 and S_2. The desired and interfering channel realizations are assumed to vary independently from one packet-exchange round to another, while the node locations, transmit powers and channel statistics remain unchanged. Therefore, the packet-delivery outcomes over the Q exchange rounds are modeled as independent trials with the same per-round success probability.

Let N_2 denote the number of fountain-coded packets generated by S_1 and successfully received by S_2 over Q exchange rounds. Since S_2 requires at least H successfully received fountain-coded packets to recover the source message, an outage occurs at S_2 when $N_2 < H$; i.e., $N_2 = 0,1, \dots, H-1$. Therefore, the outage probability at S_2 is expressed as follows:

$$\text{OP}_{S_2}^{\text{SM-3P}} = \sum_{N_2=0}^{H-1} \binom{Q}{N_2} . \left(\theta_{X_1}^{\text{SM-3P}}\right)^{N_2} \left(1 - \theta_{X_1}^{\text{SM-3P}}\right)^{Q-N_2}$$
$$= \sum_{N_2=0}^{H-1} \binom{Q}{N_2} \left(\exp(-(\lambda_{S_1 R} + \lambda_{S_2 R})\omega_2) \prod_{k=1}^{K} \frac{\lambda_{I_k R}\lambda_{I_k S_2}}{(\lambda_{I_k R} + \lambda_{S_1 R}\omega_1)(\lambda_{I_k S_2} + \lambda_{S_2 R}\omega_1)}\right)^{N_2}$$

$$\times\left(1-\exp\left(-\left(\lambda_{S_1R}+\lambda_{S_2R}\right)\omega_2\right)\prod_{k=1}^{K}\frac{\lambda_{I_kR}\lambda_{I_kS_2}}{\left(\lambda_{I_kR}+\lambda_{S_1R}\omega_1\right)\left(\lambda_{I_kS_2}+\lambda_{S_2R}\omega_1\right)}\right)^{Q-N_2}. \quad (27)$$

where $\binom{Q}{N_i}$ denotes the binomial coefficient.

Similarly, let N_1 denote the number of fountain-coded packets generated by S_2 and successfully received by S_1 over Q exchange rounds. An outage occurs at S_1 if $N_1 < H$; i.e., $N_1 = 0,1,2,\dots,H-1$. Therefore, the outage probability at S_1 is given by:

$$\mathrm{OP}_{S_1}^{\mathrm{SM-3P}} = \sum_{N_1=0}^{H-1}\binom{Q}{N_1}\left(\theta_{X_2}^{\mathrm{SM-3P}}\right)^{N_1}\left(1-\theta_{X_2}^{\mathrm{SM-3P}}\right)^{Q-N_1}$$

$$=\sum_{N_1=0}^{H-1}\binom{Q}{N_1}\left(\exp\left[-\left(\lambda_{S_1R}+\lambda_{S_2R}\right)\omega_2\right]\prod_{k=1}^{K}\frac{\lambda_{I_kR}\lambda_{I_kS_1}}{\left(\lambda_{I_kR}+\lambda_{S_2R}\omega_1\right)\left(\lambda_{I_kS_1}+\lambda_{S_1R}\omega_1\right)}\right)^{N_1}$$

$$=\sum_{N_1=0}^{H-1}\binom{Q}{N_1}\left(1-\exp\left[-\left(\lambda_{S_1R}+\lambda_{S_2R}\right)\omega_2\right]\prod_{k=1}^{K}\frac{\lambda_{I_kR}\lambda_{I_kS_1}}{\left(\lambda_{I_kR}+\lambda_{S_2R}\omega_1\right)\left(\lambda_{I_kS_1}+\lambda_{S_1R}\omega_1\right)}\right)^{Q-N_1} \quad (28)$$

2.3 TWR Model with Four Phases (SM-4P)

Similarly, because one normalized SM-4P packet-exchange round consists of four equal-duration transmission phases, the successful-decoding condition is transformed as:

$$\frac{1}{4}\log_2(1+\gamma) \ge C_{\mathrm{th}} \Leftrightarrow \log_2(1+\gamma) \ge 4C_{\mathrm{th}} \Leftrightarrow \gamma \ge 2^{4C_{\mathrm{th}}}-1 \triangleq \xi_{\mathrm{th}}.$$

The same non-strict successful-decoding convention adopted in Sub-section 2.2 is used for the SM-4P analysis. Hence, the factor four is incorporated into the SM-4P SINR threshold ξ_{th} used in the subsequent analysis.

The SM-4P-FC benchmark employs the same network topology, node locations, transmit-power definitions, CCI model, channel distributions and independent block-fading assumptions introduced in Sub-section 2.1. Unlike the two SM-3P schemes, SM-4P-FC does not perform a packet-level XOR operation at the relay. Instead, the two communication directions are forwarded separately over four transmission phases.

The corresponding four-phase transmission model is depicted in Figure 2. In the first phase, S_1 transmits its packet to R. In the second phase, R forwards the recovered packet to S_2. In the third phase, S_2 transmits its packet to R and in the fourth phase, R forwards the recovered packet to S_1. Under the common channel and interference model, the instantaneous link capacities are given by:

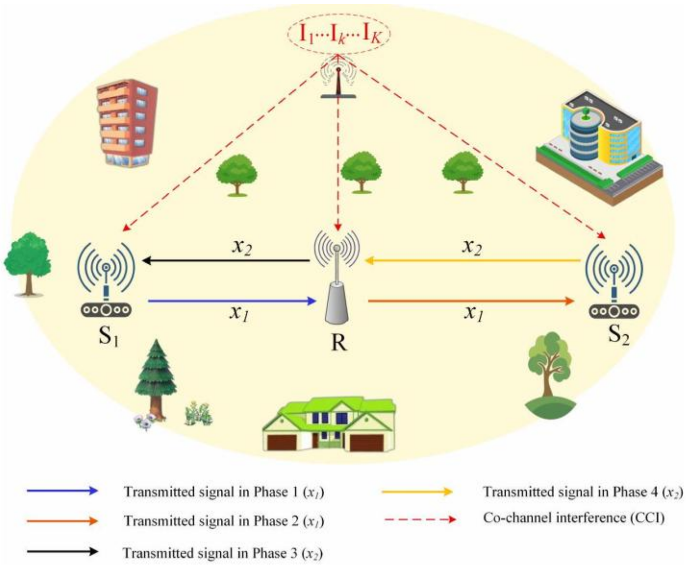

Figure 2. Four-phase TWR model operating in a co-channel interference environment.

$$C_{S_1R}=\frac{1}{4}\log_2\left(1+\frac{\Psi_S g_{S_1R}}{\sum_{k=1}^{K}\ \Psi_I g_{I_kR}+1}\right),\quad C_{RS_2}=\frac{1}{4}\log_2\left(1+\frac{\Psi_S g_{RS_2}}{\sum_{k=1}^{K}\ \Psi_I g_{I_kS_2}+1}\right),$$
$$C_{S_2R}=\frac{1}{4}\log_2\left(1+\frac{\Psi_S g_{S_2R}}{\sum_{k=1}^{K}\ \Psi_I g_{I_kR}+1}\right),\quad C_{RS_1}=\frac{1}{4}\log_2\left(1+\frac{\Psi_S g_{RS_1}}{\sum_{k=1}^{K}\ \Psi_I g_{I_kS_1}+1}\right). \tag{29}$$

Using C_{S_1R} and C_{RS_2} in Eq. (29), the per-round probability that S_2 successfully receives the encoded packet X_1 is calculated as follows:

$$\begin{aligned}\theta_{X_1}^{\mathrm{SM-4P}}&=\Pr\left(\frac{1}{4}\log_2\left(1+\frac{\Psi_S g_{S_1R}}{\sum_{k=1}^{K}\ \Psi_I g_{I_kR}+1}\right)\geq C_{\mathrm{th}}\right)\Pr\left(\frac{1}{4}\log_2\left(1+\frac{\Psi_S g_{RS_2}}{\sum_{k=1}^{K}\ \Psi_I g_{I_kS_2}+1}\right)\geq C_{\mathrm{th}}\right)\\&=\Pr\left(\frac{\Psi_S g_{S_1R}}{\sum_{k=1}^{K}\ \Psi_I g_{I_kR}+1}\geq \xi_{\mathrm{th}}\right)\Pr\left(\frac{\Psi_S g_{RS_2}}{\sum_{k=1}^{K}\ \Psi_I g_{I_kS_2}+1}\geq \xi_{\mathrm{th}}\right)\\&=\exp\left[-\left(\lambda_{S_1R}+\lambda_{S_2R}\right)\vartheta_2\right]\prod_{k=1}^{K}\frac{\lambda_{I_kR}\lambda_{I_kS_2}}{\left(\lambda_{I_kR}+\lambda_{S_1R}\vartheta_1\right)\left(\lambda_{I_kS_2}+\lambda_{S_2R}\vartheta_1\right)}.\end{aligned}\tag{30}$$

where $\vartheta_1=\xi_{\mathrm{th}}\Psi_I/\Psi_S$ and $\vartheta_2=\xi_{\mathrm{th}}/\Psi_S$.

Next, the per-round probability that S_1 successfully receives packet X_2 is calculated as:

$$\begin{aligned}\theta_{X_2}^{\mathrm{SM-4P}}&=\Pr\left(\frac{1}{4}\log_2\left(1+\frac{\Psi_S g_{S_2R}}{\sum_{k=1}^{K}\ \Psi_I g_{I_kR}+1}\right)\geq C_{\mathrm{th}}\right)\times\Pr\left(\frac{1}{4}\log_2\left(1+\frac{\Psi_S g_{RS_1}}{\sum_{k=1}^{K}\ \Psi_I g_{I_kS_1}+1}\right)\geq C_{\mathrm{th}}\right)\\&=\Pr\left(\frac{\Psi_S g_{S_2R}}{\sum_{k=1}^{K}\ \Psi_I g_{I_kR}+1}\geq \xi_{\mathrm{th}}\right)\Pr\left(\frac{\Psi_S g_{RS_1}}{\sum_{k=1}^{K}\ \Psi_I g_{I_kS_1}+1}\geq \xi_{\mathrm{th}}\right)\\&=\exp\left[-\left(\lambda_{S_1R}+\lambda_{S_2R}\right)\vartheta_2\right]\prod_{k=1}^{K}\frac{\lambda_{I_kR}\lambda_{I_kS_1}}{\left(\lambda_{I_kR}+\lambda_{S_2R}\vartheta_1\right)\left(\lambda_{I_kS_1}+\lambda_{S_1R}\vartheta_1\right)}.\end{aligned}\tag{31}$$

Finally, the outage probabilities at S_1 and S_2 under the SM-4P protocol are calculated as follows:

$$\begin{aligned}\mathrm{OP}_{S_1}^{\mathrm{SM-4P}}&=\sum_{N_1=0}^{H-1}\binom{Q}{N_1}\left(\theta_{X_2}^{\mathrm{SM-4P}}\right)^{N_1}\left(1-\theta_{X_2}^{\mathrm{SM-4P}}\right)^{Q-N_1}\\&=\sum_{N_1=0}^{H-1}\binom{Q}{N_1}\left(\exp\left[-\left(\lambda_{S_1R}+\lambda_{S_2R}\right)\vartheta_2\right]\prod_{k=1}^{K}\frac{\lambda_{I_kR}\lambda_{I_kS_1}}{\left(\lambda_{I_kR}+\lambda_{S_2R}\vartheta_1\right)\left(\lambda_{I_kS_1}+\lambda_{S_1R}\vartheta_1\right)}\right)^{N_1}\\&\times\left(1-\exp\left[-\left(\lambda_{S_1R}+\lambda_{S_2R}\right)\vartheta_2\right]\prod_{k=1}^{K}\frac{\lambda_{I_kR}\lambda_{I_kS_1}}{\left(\lambda_{I_kR}+\lambda_{S_2R}\vartheta_1\right)\left(\lambda_{I_kS_1}+\lambda_{S_1R}\vartheta_1\right)}\right)^{Q-N_1}.\end{aligned}\tag{32}$$

$$\begin{aligned}\mathrm{OP}_{S_2}^{\mathrm{SM-4P}}&=\sum_{N_2=0}^{H-1}\binom{Q}{N_2}\left(\theta_{X_1}^{\mathrm{SM-4P}}\right)^{N_2}\left(1-\theta_{X_1}^{\mathrm{SM-4P}}\right)^{Q-N_2}\\&=\sum_{N_2=0}^{H-1}\binom{Q}{N_2}\left(\exp\left[-\left(\lambda_{S_1R}+\lambda_{S_2R}\right)\vartheta_2\right]\prod_{k=1}^{K}\frac{\lambda_{I_kR}\lambda_{I_kS_2}}{\left(\lambda_{I_kR}+\lambda_{S_1R}\vartheta_1\right)\left(\lambda_{I_kS_2}+\lambda_{S_2R}\vartheta_1\right)}\right)^{N_2}\\&\times\left(1-\exp\left[-\left(\lambda_{S_1R}+\lambda_{S_2R}\right)\vartheta_2\right]\prod_{k=1}^{K}\frac{\lambda_{I_kR}\lambda_{I_kS_2}}{\left(\lambda_{I_kR}+\lambda_{S_1R}\vartheta_1\right)\left(\lambda_{I_kS_2}+\lambda_{S_2R}\vartheta_1\right)}\right)^{Q-N_2}.\end{aligned}\tag{33}$$

2.4 Sum Throughput Analysis

To complement the outage-probability analysis, we further evaluate the bandwidth-normalized throughput of the two-way relay system. Under the adopted fixed- Q, no-early-stopping packet-exchange policy, each source message contains H useful source packets and all Q packet-exchange rounds are used, even if a destination could satisfy its recovery condition before the final round. Therefore, H/Q represents the ratio between the number of useful source packets and the fixed total number of packet-exchange rounds.

For protocol $p \in \{\mathrm{SM-3P}, \mathrm{SM-4P}\}$, the throughput at terminal $S_i, i \in \{1,2\}$, is defined as:

$$\eta_{S_i}^{(p)} = \frac{H}{Q} C_{\mathrm{th}} \left(1 - \mathrm{OP}_{S_i}^{(p)}\right), \tag{34}$$

where $1 - \mathrm{OP}_{S_i}^{(p)}$ denotes the probability that terminal S_i successfully recovers the source message. Accordingly, the bidirectional sum throughput is given by:

$$\eta_{\mathrm{sum}}^{(p)} = \eta_{S_1}^{(p)} + \eta_{S_2}^{(p)} = \frac{H}{Q} C_{\mathrm{th}} \left[2 - \mathrm{OP}_{S_1}^{(p)} - \mathrm{OP}_{S_2}^{(p)}\right]. \tag{35}$$

This definition applies to the fixed- Q, no-early-stopping policy adopted for the SM-3P-FC, SM-4P-FC and SM-3P-NoFC comparisons. If early stopping were employed, the denominator would instead depend on the average number of packet-exchange rounds required for successful recovery and would require a separate analysis.

The throughput is normalized by the system bandwidth and is therefore expressed in bit/s/Hz. No additional factor of 1/3 or 1/4 is introduced in Eqs. (34 and 35), because the number of transmission phases has already been incorporated into the instantaneous capacities and the corresponding outage probabilities of the SM-3P and SM-4P protocols.

The above metric follows the ideal packet-level fountain-coding abstraction adopted in this work. Consequently, packet-header overhead, additional encoded packets required for practical decoding, decoding complexity, processing delay, memory consumption and the corresponding energy cost are not included in the throughput calculation. Therefore, the reported values represent idealized bandwidth-normalized throughput.

At the present abstraction level, practical fountain-code overhead may be approximated by evaluating the outage probabilities appearing in Eqs. (34 and 35) using an effective recovery threshold $H_{\mathrm{eff}} > H$, while retaining H/Q as the useful-payload factor. This effective-threshold substitution does not represent the complete finite-length decoding behavior. A code-specific throughput analysis would additionally require the corresponding finite-length decoding-success function, together with explicit accounting for packet-header, coding, signaling, processing, memory and energy overhead.

2.5 SM-3P Uncoded Fixed-Repetition Benchmark

To isolate the packet-recovery gain provided by fountain coding, we consider a same-budget three-phase uncoded fixed-repetition benchmark, hereafter denoted by SM-3P-NoFC. The benchmark retains the same three-phase DNC physical transmission schedule, network topology, transmit-power definitions, CCI model, channel assumptions, source-block size H and total budget of Q packet-exchange rounds as SM-3P-FC. It differs only in its packet-generation and source-message-recovery rules.

Each source message consists of H distinct uncoded packets. These packets are transmitted according to a pre-determined fixed-repetition schedule over the same Q packet-exchange rounds used by SM-3P-FC. The fixed schedule requires neither packet-level feedback nor adaptive retransmission and therefore provides a controlled same-budget comparison. It is not intended to represent all possible non-fountain coding strategies, such as feedback-based ARQ or a separate fixed-rate channel code.

Let

$$L = \left\lfloor \frac{Q}{H} \right\rfloor, r = Q - LH, \tag{36}$$

where $0 \le r < H$. For the considered benchmark, $Q \ge H$ is assumed, so that every uncoded source packet is transmitted at least once. Accordingly, r source packets are transmitted $L + 1$ times, whereas the remaining $H - r$ packets are transmitted L times. Thus, the Q transmission opportunities are distributed as evenly as possible among the H uncoded source packets.

The relay operation, DNC processing, channel model, transmit powers and interference conditions remain identical to those of the fountain-coded SM-3P protocol. Therefore, the per-round successful packet-delivery probabilities remain $\theta_{X_1}^{\mathrm{SM-3P}}$ and $\theta_{X_2}^{\mathrm{SM-3P}}$. However, without fountain coding, successful message recovery requires every one of the H distinct source packets to be received at least once. Under the adopted independent block-fading model across packet-exchange rounds, the delivery outcomes of the repeated transmissions are mutually independent.

Consequently, the outage probability at S_2 is given by:

$$\mathrm{OP}_{S_2}^{\mathrm{SM-3P-NoFC}} = 1 - \left[1 - \left(1 - \theta_{X_1}^{\mathrm{SM-3P}}\right)^{L+1}\right]^{r} \times \left[1 - \left(1 - \theta_{X_1}^{\mathrm{SM-3P}}\right)^{L}\right]^{H-r}. \quad (37)$$

Similarly, the outage probability at S_1 is:

$$\mathrm{OP}_{S_1}^{\mathrm{SM-3P-NoFC}} = 1 - \left[1 - \left(1 - \theta_{X_2}^{\mathrm{SM-3P}}\right)^{L+1}\right]^{r} \times \left[1 - \left(1 - \theta_{X_2}^{\mathrm{SM-3P}}\right)^{L}\right]^{H-r}. \quad (38)$$

When $Q = H$, each uncoded packet is transmitted once and the expressions reduce to:

$$\mathrm{OP}_{S_2}^{\mathrm{SM-3P-NoFC}} = 1 - \left(\theta_{X_1}^{\mathrm{SM-3P}}\right)^{H},$$

and

$$\mathrm{OP}_{S_1}^{\mathrm{SM-3P-NoFC}} = 1 - \left(\theta_{X_2}^{\mathrm{SM-3P}}\right)^{H}.$$

The corresponding bidirectional sum throughput is:

$$\eta_{\mathrm{sum}}^{\mathrm{SM-3P-NoFC}} = \frac{H}{Q} C_{\mathrm{th}} \left[2 - \mathrm{OP}_{S_1}^{\mathrm{SM-3P-NoFC}} - \mathrm{OP}_{S_2}^{\mathrm{SM-3P-NoFC}}\right] \quad (39)$$

This benchmark uses the same source-block size, transmission budget, three-phase protocol and DNC operation as the fountain-coded SM-3P system. Hence, the comparison isolates the benefit of allowing any H successfully received encoded packets to recover the source message, rather than requiring all H distinct uncoded packets.

3. Simulation and Analytical Results

This section presents the analytical and MC simulation results for the OPs and bidirectional sum throughputs of the SM-3P-FC, SM-3P-NoFC and SM-4P-FC schemes. The analytical curves are evaluated using the closed-form outage-probability expressions and the throughput expressions derived in Section 2, whereas the simulation results are obtained by independently generating the channel realizations and evaluating the corresponding packet-recovery events.

For consistency with the analytical notation, the labels SM-3P and SM-4P used in Figures 3-8 refer to the fountain-coded SM-3P-FC and SM-4P-FC protocols, respectively.

For each plotted point, the MC results are obtained from $N_{\mathrm{MC}} = 10^6$ independently generated channel realizations. The pseudo-random-number generator is initialized using the fixed seed 2026 with the Mersenne Twister algorithm. In all figures, analytical results are represented by continuous curves, whereas MC results are represented by discrete markers.

Unless otherwise specified, Figures 3-10 use the proportional power setting $P_S = P_I = P$ or equivalently $\Psi_S = \Psi_I = \Psi$. This setting is adopted to investigate the interference-limited behavior that occurs when the desired and interfering powers increase at the same rate. It is not an analytical restriction, because the derived expressions allow arbitrary and unequal values of Ψ_S and Ψ_I.

Figure 11 explicitly relaxes this numerical assumption by varying Ψ_S under three interference conditions: no CCI, fixed $\Psi_I = 5$ dB and proportional $\Psi_I = \Psi_S$.

For the interference-free case $K = 0$, the standard conventions $\sum_{k=1}^{0} (\cdot) = 0$ and $\prod_{k=1}^{0} (\cdot) = 1$ are adopted. The close agreement between the analytical and simulation results supports the accuracy of the derived expressions. Unless otherwise specified, the system and simulation parameters are summarized in Table 3.

For the controlled equal-large-scale-interference benchmark, the K interferers are assigned the same nominal distance profile, generated from the reference coordinate (0.3, -1.5). This controlled arrangement isolates the effect of the number of interferers while maintaining the same average large-scale propagation condition for every interferer. It is not intended to represent a literal deployment in which multiple physical interferers occupy exactly the same location. The small-scale fading coefficients associated with the K interferers are independently generated and hence their instantaneous interference contributions are independent.

Table 3. Simulation parameters and numerical settings for Figures 3-11.

Parameter	Meaning	Value or setting
S_1	Coordinate of source node S_1	(0,0)
S_2	Coordinate of source node S_2	(1,0)
R	Coordinate of relay node R	$(x_R, 0)$, where $0 < x_R < 1$
I_k	Nominal reference coordinate for the controlled equal-large-scale interference benchmark	$(0.3, -1.5), k = 1, \dots, K$
β	Path-loss exponent	3
σ_0^2	AWGN noise power at each receiving node	1
λ_{ab}	Exponential rate parameter of the channel power gain on link $a \to b$	$\lambda_{ab} = d_{ab}^{\beta}$
Fading	Small-scale fading model for the desired and interfering links	Independent block-Rayleigh fading
Channel update	Variation of the channel realizations across transmissions	Constant within one time slot and independently regenerated across time slots and exchange rounds
P_S, P_I	Desired-node and co-channel-interferer transmit powers; arbitrary in the analytical framework	$P_S = P_I = P$ for Figs. 3-10; separately specified through Ψ_S and Ψ_I for Fig. 11.
Ψ	Common normalized transmit power under $P_S = P_I = P$, where $\Psi = P/\sigma_0^2$	$0,3,6,\dots,30$ dB for Figs. 3, 4 and 10; 5 dB for Figs. 5-9.
Ψ_S, Ψ_I	Separate normalized desired-node and co-channel-interference powers used for the CCI-power comparison	For Fig. 11: $\Psi_S = 0,3,6,\dots,30$ dB; no CCI: $K = 0$; fixed CCI: $K = 2$, $\Psi_I = 5$ dB; proportional CCI: $K = 2, \Psi_I = \Psi_S$
C_{th}	Target spectral-efficiency threshold	0.1 bit/s/Hz for Figs. 3-8 and 10-11; 0.1, 0.2, . . . , 1.0 bit/s/Hz for Fig. 9.
H	Source-block size and recovery threshold for the fountain-coded schemes	3 for Figs. 3, 5, 6 and 811; 4 for Fig. 4; 4, 5, ..., 10 for Fig. 7.
Q	Maximum number of packet-exchange rounds	4 for Fig. 3; 5 for Figs. 4, 6 and 8-11; 3,4,5,6 for Fig. 5; 10 for Fig. 7.
x_R	X-coordinate of relay R on the $S_1 - S_2$ line segment	0.4 for Fig. 3; 0.75 for Fig. 4; 0.35 for Figs. 5, 711; 0.1, 0.2, . . , 0.9 for Fig. 6.
K	Number of co-channel interferers	2 for Figs. 3-6, 9 and 10; 3 for Fig. 7; 1,2,...,10 for Fig. 8; 0 or 2 for Fig. 11.
N_{MC}	Number of independently generated channel realizations for each plotted point	10^6
Random seed	Initialization of the MATLAB pseudo-random-number generator	2026, Mersenne Twister
Software	Software used for the analytical evaluations and Monte Carlo simulations	MATLAB R2024b

The numerical evaluations are conducted in a two-dimensional Cartesian coordinate system, where $S_1 = (0,0), S_2 = (1,0)$ and $R = (x_R, 0)$. All K co-channel interferers are assigned the same nominal coordinate in the reported numerical experiments. This fixed-location setting is not intended to represent a general spatial deployment. Rather, it provides a controlled conditional benchmark that isolates the impact of the number of interferers under identical large-scale propagation conditions.

With $S_1 = (0,0), S_2 = (1,0), R = (x_R, 0)$ and $I_k = (0.3, -1.5)$, the distances from each co-channel interferer to the receiving nodes are explicitly determined as: $d_{I_k S_1} = \sqrt{0.3^2 + 1.5^2}$, $d_{I_k S_2} = \sqrt{(1 - 0.3)^2 + 1.5^2}$ and $d_{I_k R} = \sqrt{(x_R - 0.3)^2 + 1.5^2}, k = 1, \dots, K$.

Accordingly, the corresponding exponential rate parameters used in the analytical and MC evaluations

Jordanian Journal of Computers and Information Technology (JJCIT), Vol. 12, No. 03, September 2026.

are $\lambda_{I_k S_1} = d^{\beta}_{I_k S_1}, \lambda_{I_k S_2} = d^{\beta}_{I_k S_2}, \lambda_{I_k R} = d^{\beta}_{I_k R}$.

Although all K interferers are assigned the same nominal coordinate in the controlled numerical benchmark, their small-scale fading coefficients are independently generated. Thus, they share the same large-scale channel parameters, but produce independent instantaneous interference contributions.

A more general deployment can incorporate randomly distributed interferers through a spatial point-process model [30]. For a fixed number K, the interferer locations may be modeled by a binomial point process within a bounded deployment region. Alternatively, a Poisson point process may be employed when both the number and locations of the active interferers within a bounded observation region are random.

Conditioned on a spatial realization Φ_I, the present link-level expressions remain applicable by assigning each interferer location $\mathbf{x}_{I_k} \in \Phi_I$ and setting $d_{I_k b} = \|\mathbf{x}_{I_k} - \mathbf{x}_b\|, \lambda_{I_k b} = d^{\beta}_{I_k b}$, for each receiving node $b \in \{R, S_1, S_2\}$. Under the adopted exponential channel-power model, this definition gives $\mathbb{E}[g_{I_k b} \mid \Phi_I] = \frac{1}{\lambda_{I_k b}} = d^{-\beta}_{I_k b}$. A spatially averaged outage probability would then be obtained as $\overline{\mathrm{OP}}_{S_i} = \mathbb{E}_{\Phi_I}[\mathrm{OP}_{S_i} \mid \Phi_I]$, which requires an additional averaging operation over the random network geometry. Such a stochastic-geometry extension is beyond the scope of the present fixed- K, fixed-location analysis.

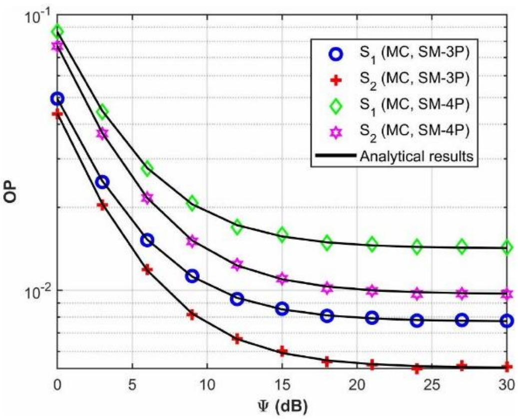

Figure 3. OP *versus* Ψ for $x_R = 0.4, H = 3, Q = 4$ and $K = 2$.

Figure 3 plots the OPs at S_1 and S_2 for the SM-3P and SM-4P protocols as functions of Ψ (in dB), with $H = 3, Q = 4$ and $K = 2$. As observed, the OP at both source nodes decreases as Ψ increases. This is because, in the low- and moderate-SNR regions, increasing Ψ improves the received signal quality and hence raises the successful packet decoding probability. However, since the interferers are also assumed to use the same transmit power scaling; i.e., $P_S = P_I = P$, the co-channel interference power increases together with the desired signal power. Therefore, at high Ψ, the system becomes interference-limited and the OP curves approach an outage floor. The figure also shows that the OPs achieved by the SM-3P scheme are always lower than those of the SM-4P scheme. This is because the three-phase protocol provides a larger pre-log factor (1/3 instead of 1/4), resulting in a higher instantaneous link capacity and, consequently, a lower outage probability. In addition, the OP at S_1 is higher than that at S_2, mainly due to the relay placement and the considered locations of the co-channel interferers.

Figure 4 plots the OPs at S_1 and S_2 for the SM-3P and SM-4P protocols as functions of Ψ, with $x_R = 0.75, H = 4, Q = 5$ and $K = 2$. Similar to Figure 3, the OPs initially decrease as Ψ increases and subsequently approach non-zero outage floors. This behavior occurs, because the desired nodes and co-channel interferers use the same power scaling; i.e., $P_S = P_I = P$, causing the system to become interference-limited at high Ψ.

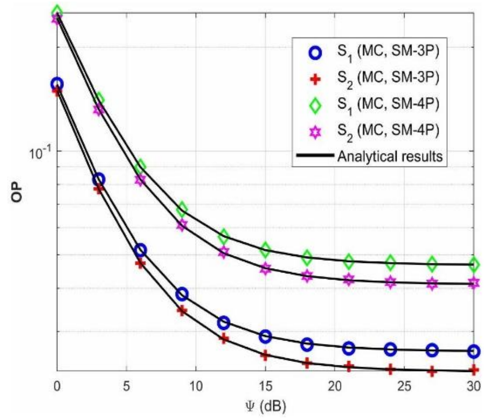

Figure 4. OP *versus* Ψ for $x_R = 0.75, H = 4, Q = 5$ and $K = 2$.

The SM-3P protocol consistently achieves lower OPs than the SM-4P protocol, because its larger pre-log factor results in a lower SINR threshold for the same target spectral efficiency. The difference between the OPs at S_1 and S_2 is primarily caused by the asymmetric relay and interferer geometry. Compared with Figure 3, relocating the relay to $x_R = 0.75$ changes the balance between the two end-to-end communication directions, whereas the different values of H and Q mainly affect the overall message-recovery probability.

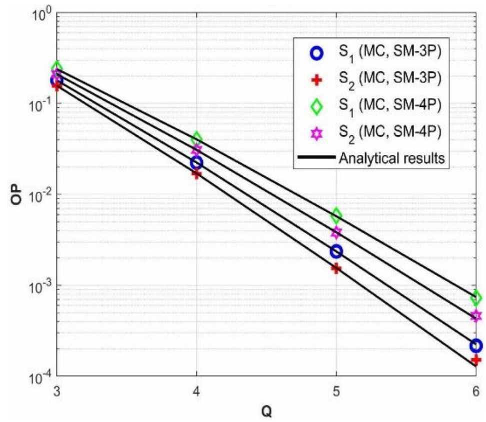

Figure 5. OP *versus* Q for $\Psi = 5$ dB$, x_R = 0.35, H = 3$ and $K = 2$.

Figure 5 plots the OPs at S_1 and S_2 for the SM-3P and SM-4P protocols as functions of the number of exchange rounds Q, with $\Psi = 5$ dB$, x_R = 0.35, H = 3$ and $K = 2$. It can be observed that the OPs at both source nodes under the SM-3P scheme remain lower than those under the SM-4P scheme. This is because the analyzed SM-3P protocol uses a larger pre-log factor than the four-phase protocol, resulting in a higher instantaneous link capacity and, consequently, a higher successful packet-decoding probability. The figure also shows that the OP at both S_1 and S_2 decreases as Q increases. This is because a larger Q increases the likelihood that the source nodes can successfully collect at least H fountain-coded packets required for successful message recovery, thereby reducing the outage probability. It is worth noting that the horizontal axis starts from $Q = 3$, because $H = 3$ is fixed in this experiment. Since at least H successfully received fountain-coded packets are required for message recovery, the cases with $Q < H$ are trivial, as successful recovery is impossible and the outage probability becomes unity. Therefore, only the meaningful region $Q \geq H$ is presented in the figure.

Figure 6 plots the OPs at S_1 and S_2 for the SM-3P and SM-4P protocols as functions of the relay location x_R, with $\Psi = 5$ dB$, Q = 5, H = 3$ and $K = 2$. It can be observed that the relay location has a pronounced impact on the outage performance of both source nodes. As x_R varies, the distances of the two hops change simultaneously, so improving one source-to-relay link may degrade the corresponding relay-to-source link on the other side. Therefore, a trade-off arises between the two transmission hops, which leads to a non-monotonic OP behavior. As a result, there exists an optimal relay region in which the OP of the source nodes is minimized.

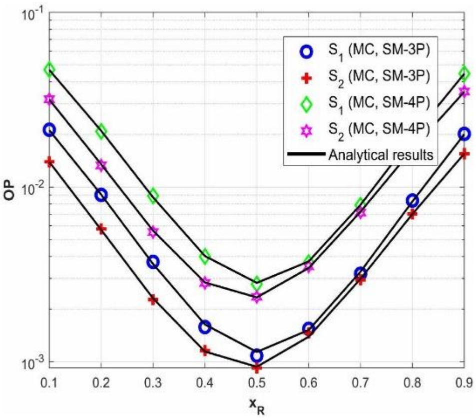

Figure 6. OP *versus* x_R for $\Psi = 5$ dB, $Q = 5, H = 3$ and $K = 2$.

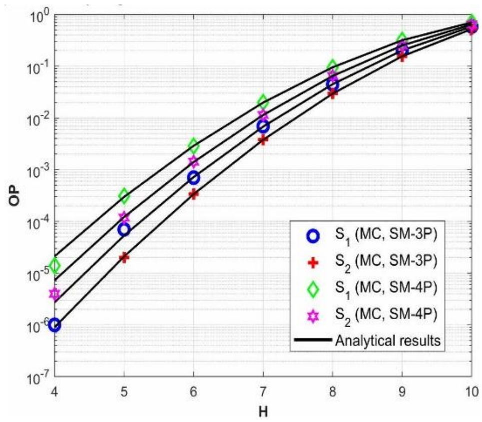

Figure 7. OP versus H for $\Psi = 5$ dB, $Q = 10, x_R = 0.35$ and $K = 3$.

Figure 7 shows the OPs at S_1 and S_2 as functions of the recovery threshold H. For a fixed $Q = 10$, the OPs increase as H increases, because a larger number of successfully received fountaincoded packets is required for source-message recovery. Therefore, the probability of collecting an insufficient number of packets becomes higher. The SM-3P protocol consistently achieves lower OPs than the SM-4P protocol over the entire considered range, further demonstrating the reliability advantage of the three-phase transmission structure.

The horizontal axis starts from $H = 4$, because $H = 3$ is used as the baseline recovery threshold in Figures 3, 5, 6 and 8-11, whereas Figure 7 focuses on stricter message-recovery requirements. All considered values satisfy $H \leq Q = 10$.

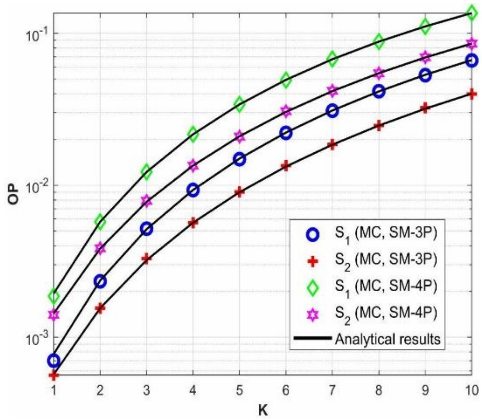

Figure 8. OP *versus* K for $\Psi = 5$ dB, $Q = 5, x_R = 0.35$ and $H = 3$.

Figure 8 plots the OPs at S_1 and S_2 for the SM-3P and SM-4P protocols as functions of K, with $\Psi = 5$ dB, $Q = 5, x_R = 0.35$ and $H = 3$. As observed, the OP at both nodes increases as K increases. This is because a larger number of co-channel interferers causes more severe interference on the transmission links, which reduces the received SINR and, consequently, the successful decoding probability of fountain-coded packets. Therefore, the probability that the sources fail to collect the required H packets becomes higher, resulting in a larger OP. The figure also shows that the OPs achieved by the SM-3P scheme are always lower than those of the SM-4P scheme, confirming the effectiveness of the analyzed SM-3P protocol under stronger co-channel interference.

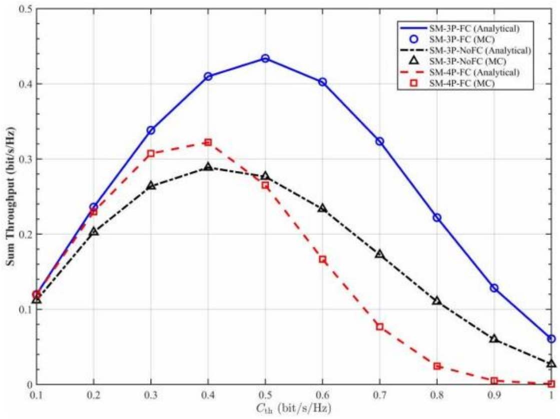

Figure 9. Bidirectional sum throughput *versus* C_{th} for the SM-3P-FC, SM-3P-NoFC and SM-4P-FC schemes with $\Psi = 5$ dB, $H = 3$, $Q = 5$, $x_R = 0.35$ and $K = 2$.

Figure 9 compares the bidirectional sum throughputs of the SM-3P-FC, SM-3P-NoFC and SM-4P-FC schemes as functions of C_{th} . Close agreement is observed between the analytical curves and the Monte Carlo markers over the evaluated C_{th} grid, supporting the accuracy of the derived throughput expressions, including the newly introduced SM-3P-NoFC benchmark. The maximum absolute deviations between the analytical and MC results over the evaluated C_{th} grid are $4.558 \times 10^{-4}, 2.345 \times 10^{-4}$ and 2.890×10^{-4} for SM-3P-FC, SM-3P-NoFC and SM-4P-FC, respectively. These maximum deviations occur at $C_{\mathrm{th}} = 0.6$,0.6 and 0.7 bit/s/Hz, respectively.

For all three schemes, the sum throughput initially increases with C_{th}, reaches a maximum and then decreases. At small C_{th}, the increase in spectral efficiency dominates the corresponding reliability loss. At larger C_{th} , however, the increased SINR threshold causes a rapid increase in outage probability and the reliability loss outweighs the spectral-efficiency improvement.

Under the common Figure 9 setting and over the evaluated target-spectral-efficiency grid $C_{\mathrm{th}} \in \{0.1, 0.2, \ldots, 1.0\}$ bit $/\mathrm{s/Hz}$, the analytical SM-3P-FC curve reaches its maximum evaluated sum throughput of approximately 0.433753 bit/s/Hz at $C_{\mathrm{th}} = 0.5$ bit/s/Hz. By comparison, the analytical SM-3P-NoFC and SM-4P-FC curves reach their corresponding maxima of approximately 0.288574 and 0.322001 bit/s/Hz, respectively, at $C_{\mathrm{th}} = 0.4 \mathrm{bit/s/Hz}$. Accordingly, within the considered numerical setting, the maximum analytical throughput of SM-3P-FC is approximately 50.3% higher than that of SM-3P-NoFC and approximately 34.7% higher than that of SM-4P-FC.

The SM-4P-FC scheme outperforms the SM-3P-NoFC benchmark at relatively small values of C_{th} , indicating that the recovery flexibility provided by fountain coding may compensate for the additional transmission phase in this region. However, for the sampled points satisfying $C_{\mathrm{th}} \geq 0.5$ bit/s/Hz, SM-3P-NoFC outperforms SM-4P-FC, because the lower SINR threshold associated with the three-phase structure becomes increasingly important. These results demonstrate that both fountain coding and the reduction in the number of transmission phases contribute to the throughput improvement of the proposed SM-3P-FC scheme.

To further isolate the reliability contributions of fountain coding and the three-phase transmission structure, Figure 10 compares the OPs of the SM-3P-FC, SM-3P-NoFC and SM-4P-FC schemes.

The analytical curves are in close agreement with the MC markers for all three schemes at both terminals. The maximum absolute MC-analytical deviation among the six plotted cases is below 7.22×10^{-4}, further validating the newly introduced SM-3P-NoFC outage expressions.

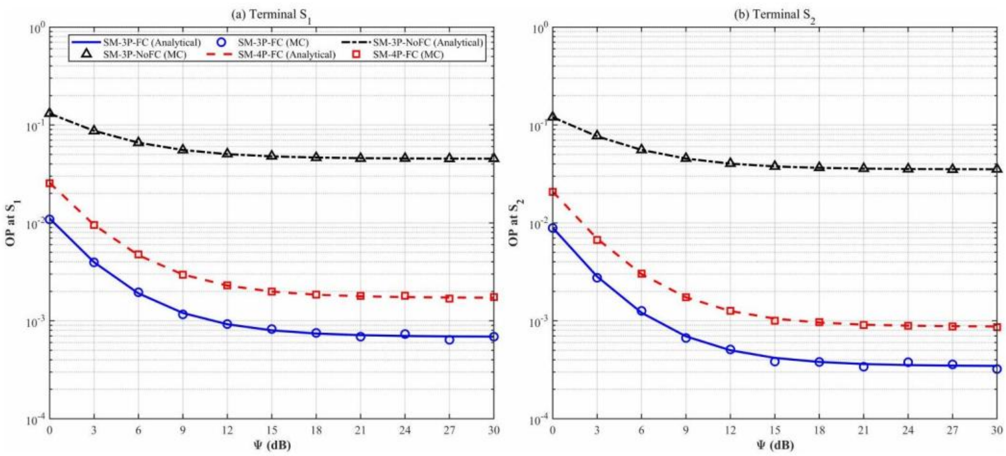

Figure 10. Outage probability of the SM-3P-FC, SM-3P-NoFC and SM-4P-FC schemes *versus* Ψ at (a) S_1 and (b) S_2, with $C_{\text{th}} = 0.1\text{bit/s/Hz}, H = 3, Q = 5, x_R = 0.35$ and $K = 2$.

Over the entire considered normalized transmit-power range, the SM-3P-FC scheme achieves the lowest OP at both terminals, whereas the SM-3P-NoFC benchmark exhibits the highest OP. The ordering is therefore $\text{OP}^{\text{SM-3P-FC}} < \text{OP}^{\text{SM-4P-FC}} < \text{OP}^{\text{SM-3P-NoFC}}$.

The comparison between SM-3P-FC and SM-3P-NoFC directly demonstrates the recovery advantage provided by fountain coding, whereas the comparison between SM-3P-FC and SM-4P-FC quantifies the reliability gain obtained by reducing the number of transmission phases. As Ψ increases, all three schemes approach non-zero outage floors, because the desired and interfering powers are increased proportionally under $P_S = P_I = P$.

Figure 8 has quantified the effect of the number of co-channel interferers. To complement that result and isolate the effect of the interference-power scaling rule, Figure 11 compares the proposed SM-3P-FC scheme under interference-free, fixed-power CCI and proportional-power CCI conditions. The analytical curves closely agree with the MC markers under all three interference conditions. The maximum absolute MC-analytical deviation among the six evaluated cases is below 2.25×10^{-4}, confirming the validity of the derived expressions for unequal values of Ψ_S and Ψ_I, as well as for the interference-free case $K = 0$. At high desired-node powers, several empirical OP values are zero, because no outage event is observed among the $N_{\text{MC}} = 10^6$ channel realizations. These zero-valued MC points are therefore omitted from the logarithmic plots.

Figure 11 demonstrates that both the presence of CCI and the manner in which its power scales with the desired-node transmit power have substantial effects on the outage behavior. In the interference-free case, the OPs at both terminal nodes decrease rapidly as Ψ_S increases, because only thermal noise and the desired-link fading affect packet delivery.

When the interference power is fixed at $\Psi_I = 5$ dB, the OPs are higher than those in the interference-free case, particularly in the low- and moderate- Ψ_S regions. Nevertheless, the OPs continue to decrease as Ψ_S increases. This behavior follows from $\omega_1 = \frac{\rho_{\text{th}}\Psi_I}{\Psi_S} \to 0$ and $\omega_2 = \frac{\rho_{\text{th}}}{\Psi_S} \to 0$, when Ψ_I remains fixed and Ψ_S increases.

By contrast, when the desired and interfering powers increase proportionally; i.e., $\Psi_I = \Psi_S$, the ratio Ψ_I/Ψ_S remains constant and $\omega_1 = \rho_{\text{th}}$. Consequently, the improvement obtained by increasing Ψ_S gradually saturates and the OPs approach non-zero interference-limited floors. Across the entire considered range, the interference-free case provides the lowest OP. When $\Psi_S < 5$ dB, the fixed-power CCI case may exhibit a higher OP than the proportional-power case, because the fixed interference power exceeds the desired-node power. The two CCI conditions would coincide at $\Psi_S = 5$ dB, where the fixed interference power equals the desired-node transmit power. For $\Psi_S > 5$ dB, the fixed-power CCI becomes progressively weaker relative to the desired signal, whereas the proportional-power CCI remains equally strong in relative terms and ultimately produces a non-zero outage floor.

Across both terminal nodes and all three interference scenarios, the global maximum absolute deviation between the analytical and Monte Carlo outage probabilities is approximately $2.243 \times$

10^{-4}. This maximum deviation occurs at terminal S_2 under the fixed-power CCI setting. The close agreement between the analytical and Monte Carlo results supports the accuracy of the derived outage-probability expressions over the evaluated desired-power range.

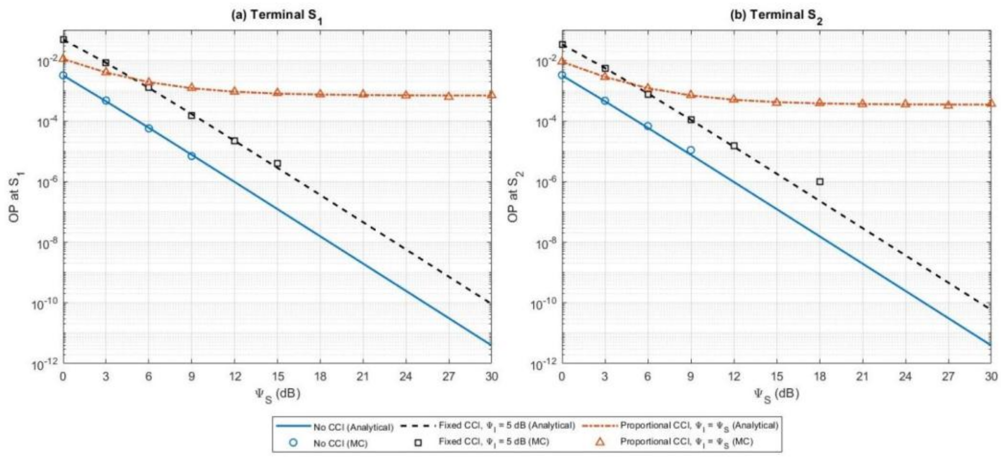

Figure 11. Effect of CCI power scaling on the outage probability of SM-3P-FC at (a) S_1 and (b) S_2: no CCI ($K = 0$), fixed CCI ($K = 2, \Psi_I = 5$ dB) and proportional CCI ($K = 2, \Psi_I = \Psi_S$).

At relatively high desired-node powers, several Monte Carlo outage estimates in the interference-free and fixed-power CCI cases become zero, because no outage event is observed among the $N_{\mathrm{MC}} = 10^6$ generated channel realizations. Since zero-valued samples cannot be displayed on a logarithmic scale, the corresponding MC markers are omitted from Figure 11. These zero-valued estimates reflect the finite Monte Carlo resolution rather than an analytical claim of exactly zero outage probability.

Engineering design implications: The numerical results provide several guidelines for the design of fountain-coded two-way relay networks operating under co-channel interference. First, increasing the desired-node transmit power cannot eliminate the outage floor when the interference power follows the same scaling. Under proportional scaling of P_S and P_I, the ratio Ψ_I/Ψ_S remains constant and the system remains interference-limited. By contrast, when P_S increases while P_I remains bounded, the desired-to-interference power ratio improves and the outage probability continues to decrease. Therefore, desired-node power allocation should be combined with interference-aware scheduling and interference suppression rather than uniformly increasing the powers of all transmitting nodes.

Second, the relay position should be selected by considering both desired link distances and the exposure of the relay and source nodes to the co-channel interferers. Placing the relay closer to one source can improve the corresponding hop while degrading the opposite communication direction, which may produce unequal outage probabilities at S_1 and S_2. Hence, a balanced relay placement should minimize the worst outage probability of the two end nodes rather than optimizing only one link.

Third, the fountain-code parameters H and Q introduce a reliability-latency trade-off. For a fixed H, increasing Q gives the destinations more opportunities to collect the required encoded packets and therefore reduces the outage probability, but it also increases the maximum delivery delay and the number of transmission rounds. In contrast, for a fixed Q, increasing H imposes a stricter recovery requirement and generally increases the outage probability. Thus, H and Q should be jointly selected according to the required reliability and latency constraints of the considered WSN application.

Finally, the performance degradation caused by a larger number of co-channel interferers indicates that the analyzed SM-3P-FC scheme is most beneficial when combined with appropriate interference control. The three-phase structure reduces the packet exchange by one time slot compared with the conventional four-phase protocol, but its practical reliability still depends on the number and locations of the interferers, the relay placement and the selected fountain-code parameters. The reported results are conditioned on the fixed interference geometry specified in Table 3. In deployments with randomly located interferers, the reliability may also vary substantially across spatial realizations, because the relay and the two terminal nodes can experience different aggregate interference levels.

4. CONCLUSIONS AND FUTURE DIRECTIONS

This paper investigated the outage and sum-throughput performance of a three-phase two-way relay network that combines fountain coding and packet-level digital network coding in the presence of co-channel interference. The considered SM-3P-FC protocol reduces the packet exchange from four time slots in the conventional SM-4P-FC protocol to three time slots by combining the relay broadcast operation with digital network coding. Closed-form expressions for the packet-delivery probabilities and the resulting outage probabilities at both terminal nodes were derived over independent block-Rayleigh fading channels. Based on these results, a bandwidth-normalized bidirectional sum-throughput expression was also developed to characterize the reliability-rate trade-off.

The analytical results were validated through Monte Carlo simulations using 10^6 independently generated channel realizations per plotted point. The close agreement between the analytical curves and simulation markers supports the accuracy of the derived outage-probability and throughput expressions. The numerical results show that the SM-3P-FC scheme consistently achieves lower outage probabilities and higher sum throughput than the SM-4P-FC scheme under the considered system configurations. When the desired and interfering transmit powers increase proportionally, the system becomes interference-limited and the outage probabilities approach non-zero floors. The additional CCI-power comparison further shows that the outage probabilities continue to decrease when interference is absent or when its power remains fixed, whereas proportional desired/interference power scaling produces non-zero outage floors. The results further demonstrate that relay placement, the recovery threshold H, the maximum number of exchange rounds Q and the number of co-channel interferers K have significant effects on system reliability. In addition, the sum throughput first increases and then decreases with the target spectral efficiency, revealing an optimum operating rate for each protocol.

These findings provide several practical design implications. Increasing the desired-node transmit power alone cannot eliminate the outage floor when the interference power follows the same scaling. Relay placement should therefore be selected by considering the reliability of both communication directions rather than optimizing only one link. Hence, the coding strategy, number of transmission phases and fountain-code parameters H, Q and C_{th} should be jointly selected according to the required reliability, latency and throughput constraints.

Under the common Figure 9 setting and over the evaluated target-spectral-efficiency grid $C_{\text{th}} \in \{0.1, 0.2, . . . , 1.0\}$ bit/s/Hz, the maximum evaluated bidirectional sum throughputs of the SM-3P-FC, SM-3P-NoFC and SM-4P-FC schemes are approximately 0.434, 0.289 and 0.322 bit/s/Hz, respectively. Accordingly, within the considered numerical setting, the maximum evaluated throughput of SM-3P-FC is approximately 50.3% higher than that of SM-3P-NoFC and approximately 34.7% higher than that of SM-4P-FC. The outage-probability comparison further shows that SM-3P-FC achieves the lowest outage probability among the three schemes over the considered normalized transmit-power range. These findings separately demonstrate the benefits of fountain coding and the reduction in the number of transmission phases.

Coding-assisted cooperative communication has also been investigated for WSNs using LDPC/OFDM approaches [39], supporting the broader relevance of channel coding in resource-constrained cooperative networks.

The present analysis adopts an ideal packet-level fountain-coding model and assumes fixed node locations and independent block-Rayleigh fading. Equal desired and interfering transmit powers are used in Figures 3-10, whereas Figure 11 considers interference-free, fixed-interference power and proportional-power settings. Future work may consider specific practical fountain-code constructions and degree distributions, finite-length decoding overhead, effective recovery thresholds and decoding-complexity-aware performance analysis for resource-constrained WSN nodes. Other useful extensions include separate source and relay power allocation together with interference-management mechanisms under energy and interference constraints; binomial- and Poisson-point-process models for randomly distributed co-channel interferers, together with spatially averaged outage and throughput analyses; more general fading models, such as Rician and Nakagami- m fading; imperfect channel-state information; spatially correlated channels; and multi-relay extensions employing sum-rate-based relay selection and adaptive relay placement.

Prior studies have shown that sum-rate-based selection can outperform max-min or end-to-end selection in the corresponding half/full-duplex two-way relaying models [40][41][42]. Future extensions should also account for feedback delay and channel-estimation error, since these impairments may reduce the achievable diversity order and coding gain. Security-oriented extensions may further investigate the impact of feedback delay on the secrecy performance of half/full duplex two-way relaying [43]. Additional communication metrics, such as delay, energy efficiency, bit-error rate and ergodic capacity, may also be considered.

REFERENCES

[1] J. N. Laneman, D. Tse and G. W. Wornell, “Cooperative Diversity in Wireless Networks: Efficient Protocols and Outage Behavior,” IEEE Transactions on Information Theory, vol. 50, no. 12, pp. 3062-3080, 2004.

[2] R. Ahlswede, N. Cai, S.-Y. Li and R. W. Yeung, “Network Information Flow,” IEEE Transactions on Information Theory, vol. 46, no. 4, pp. 1204-1216, DOI: 10.1109/18.850663, 2000.

[3] W. Han, S. Xu, D. Huang and C. Xu, “Analysis and Design of Rateless Two-way Relay Networks Based on a Multiply-and-forward Scheme,” Applied Sciences, vol. 10, no. 7, Article no. 2389, 2020.

[4] P. N. Son and T. T. Duy, “A New Approach for Two-way Relaying Networks: Improving Performance by Successive Interference Cancellation, Digital Network Coding and Opportunistic Relay Selection,” Wireless Networks, vol. 26, no. 2, pp. 1315-1329, DOI: 10.1007/s11276-019-02186-1, 2020.

[5] D. R. Pattanayak, V. K. Dwivedi and V. Karwal, “Physical Layer Security of a Two Way Relay Based Mixed FSO/RF Network in the Presence of Multiple Eavesdroppers,” Optics Communications, vol. 463, Article no. 125429, DOI: 10.1016/j.optcom.2020.125429, 2020.

[6] T.-T. T. Nguyen and D.-T. Do, “Exploiting Performance of Two-way Non-orthogonal Multiple Access Networks: Joint Impact of Co-channel Interference, Full-duplex/Half-duplex Mode and SIC Receiver,” Ad Hoc Networks, vol. 97, Article no. 102032, DOI: 10.1016/j.adhoc.2019.102032, 2020.

[7] P. M. Nam et al., “Outage Performance of Interference Cancellation-aided Two-way Relaying Cognitive Network with Primary TAS/SC Communication and Secondary Partial Relay Selection,” Electronics, vol. 11, no. 22, Article no. 3645, DOI: 10.3390/electronics11223645, 2022.

[8] V. Ozduran and E. Soleimani-Nasab, “Multi-user Two-way Relaying in the Presence of Co-channel Interference,” IET Communications, vol. 14, no. 21, pp. 3853-3865, DOI: 10.1049/iet-com.2020.0170, 2020.

[9] T. T. Duy et al., “Outage Probability of Interference Cancellation Based Two-way Relaying Cognitive Radio Protocol with Primary MIMO Communication,” Proc. Of the 2020 IEEE 8th Int. Conf. on Communications and Electronics (ICCE), pp. 481-486, DOI: 10.1109/ICCE48956.2021.9352135, 2021.

[10] D. Sun, Z. Liu and X. Zhang, “Dynamic Cooperative Communications with Mutual Information Accumulation for Mobile Robots in Industrial Internet of Things,” Sensors, vol. 24, no. 13, p. 4362, 2024.

[11] N. Q. Sang et al., “On the Security and Reliability Trade-off of the Satellite Terrestrial Networks with Fountain Codes and Friendly Jamming,” EAI Endorsed Transactions on Industrial Networks and Intelligent Systems, vol. 10, no. 4, e3, DOI: 10.4108/eetinis.v10i4.4192, 2023.

[12] G. Huang et al., “Improving Throughput in SWIPT-based Wireless Multi-relay Networks with Relay Selection and Rateless Codes,” Digital Communications and Networks, vol. 10, no. 4, pp. 1131-1144, 2024.

[13] H. Shao, H. Zhu and J. Bao, “Analysis and Design of Enhanced Distributed Fountain Codes in Multiple Access Networks with Cooperative Relay,” Symmetry, vol. 14, Article no. 2026, DOI: 10.3390/sym14102026, 2022.

[14] V. T. Nguyen et al., “On Performance Evaluation of Hybrid Satellite-terrestrial Relaying Networks with Fountain Coding, NOMA and RIS,” REV J. on Electronics and Communi., vol. 15, no. 3, pp. 113-124, 2025.

[15] N. V. Toan et al., “Security-reliability Analysis of NOMA-assisted Hybrid Satellite-terrestrial Relay Multi-cast Transmission Networks Using Fountain Codes and Partial Relay Selection with Presence of Multiple Eavesdroppers,” EAI Endorsed Trans. On Industrial Networks and Intelligent Systems, vol. 12, no. 3, DOI: 10.4108/eetinis.v12i3.8604, 2025.

[16] S. Atapattu et al., “Reconfigurable Intelligent Surface Assisted Two-way Communications: Performance Analysis and Optimization,” IEEE Trans. On Communications, vol. 68, no. 10, pp. 6552-6567, 2020.

[17] J. Wang, Y.-C. Liang, J. Joung, X. Yuan and X. Wang, “Joint Beamforming and Reconfigurable Intelligent Surface Design for Two-way Relay Networks,” IEEE Trans. On Communi., vol. 69, no. 8, pp. 5620-5633, 2021.

[18] H. Sun, F. Han, S. Zhao and H. Deng, “Optimal Energy-harvesting Design for AF and DF Two-way Relay Beamforming in 6G,” EURASIP J. on Wireless Communi. And Networking, vol. 2022, Article no. 73, 2022.
[19] K. Zhong and L. Fu, “Throughput Maximization for the Full-duplex Two-way Relay System with Energy Harvesting,” Electronics, vol. 12, no. 1, Article no. 16, DOI: 10.3390/electronics12010016, 2023.
[20] H. T. Nguyen et al., “Fountain Coding Based Two-way Relaying Cognitive Radio Networks Employing Reconfigurable Intelligent Surface and Energy Harvesting,” Telecom, vol. 6, no. 1, Article no. 1, 2025.
[21] C. Bian, Y. Shao, H. Wu and D. Gündüz, “Deep Joint Source-channel Coding over the Relay Channel,” Proc. Of the 2024 IEEE Int. Conf. on Machine Learning for Communication and Networking (ICMLCN), pp. 139-144, DOI: 10.1109/ICMLCN59089.2024.10624800, 2024.
[22] C. Bian et al., “Process-and-forward: Deep Joint Source-channel Coding over Cooperative Relay Networks,” IEEE Journal on Selected Areas in Communications, vol. 43, no. 4, pp. 1118-1134, 2025.
[23] T. T. Duy and H. Y. Kong, “Exact Outage Probability of Cognitive Two-way Relaying Scheme with Opportunistic Relay Selection under Interference Constraint,” IET Comm., vol. 6, no. 16, pp. 2750-2759, 2012.
[24] T.-A. Ngo et al., “Half-duplex Two-way Relaying for Wireless Sensor Networks with Adaptive Coding Rate: A Performance Optimization Framework,” Journal of Telecomm. And Inf. Tech., vol. 102, no. 4, pp. 69-76, 2025.
[25] D.-H. Ha et al., “Security and Reliability Analysis of a Two-way Half-duplex Wireless Relaying Network Using Partial Relay Selection and Hybrid TPSR Energy Harvesting at Relay Nodes,” IEEE Access, vol. 8, pp. 187165-187181, DOI: 10.1109/ACCESS.2020.3030794, 2020.
[26] N. T. Hau, P. M. Nam, P. T. Tin, T. T. Duy and T. Hanh, “Outage Performance of Two-way Relaying Secure Multicast Networks Using Fountain Codes and Digital Network Coding,” Proc. Of the 7th Int. Conf. on Green Techn. And Sustainable Development (GTSD), pp. 528-532, DOI: 10.1109/GTSD62346.2024.10674819, 2024.
[27] N. V. Toan, N. T. Hau, P. M. Nam, P. N. Son and T. T. Duy, “Analysis of Security-reliability Tradeoff of Two-way Hybrid Satellite-terrestrial Relay Schemes Using Fountain Codes, Successive Interference Cancelation, Digital Network Coding, Partial Relay Selection and Cooperative Jamming,” Telecom, vol. 7, no. 1, Article no. 5, DOI: 10.3390/telecom7010005, 2026
[28] A. Shokrollahi, “Raptor codes,” IEEE Transactions on Information Theory, vol. 52, no. 6, pp. 2551-2567, DOI: 10.1109/TIT.2006.874390, 2006.
[29] M. Luby, “LT Codes,” Proc. Of the 43rd Annual IEEE Symposium on Foundations of Computer Science (FOCS), pp. 271-280, DOI: 10.1109/SFCS.2002.1181950, 2002.
[30] M. Haenggi, Stochastic Geometry for Wireless Networks, Cambridge University Press, DOI: 10.1017/CBO9781139043816, 2012.
[31] V. Ozduran, J. M. Cioffi and S. B. Yarman, “Opportunistic Source-pair Selection (OSPS) Method for Multiuser Bi-directional Wireless Relaying Networks,” Proc. Of the 2013 IEEE 14th Workshop on Signal Processing Advances in Wireless Communications (SPAWC), pp. 565-569, DOI: 10.1109/SPAWC.2013.6612113, 2013.
[32] V. Ozduran, E. Soleimani-Nasab and B. S. Yarman, “Opportunistic Source-pair Selection for Multi-user Two-Way Amplify-and-forward Wireless Relaying Networks,” IET Comm., vol. 10, no. 16, pp. 2106-2118, 2016.
[33] V. Ozduran, B. S. B. Yarman and J. M. Cioffi, “Opportunistic Source-pair Selection Method with Imperfect Channel State Information for Multiuser Bi-directional Relaying Networks,” IET Communications, vol. 13, no. 7, pp. 905-917, DOI: 10.1049/iet-com.2018.5129, 2019.
[34] V. Ozduran, N. H. Mahmood and N. Nomikos, “Performance Analysis of Power-domain Non-orthogonal Multiple Access for Full-duplex Two-way Relaying,” Transactions on Emerging Telecommunications Technologies, vol. 33, no. 7, Article no. e4487, DOI: 10.1002/ett.4487, 2022.
[35] V. Ozduran, “Secrecy Achievable Rate of Two-way Illegitimate Full-duplex Relay-assisted NOMA with CCI,” Wireless Personal Communications, vol. 132, pp. 865-888, DOI: 10.1007/s11277-023-10640-9, 2023.
[36] V. Ozduran et al., “Impact of Co-channel Interference on Sum-rate-based Opportunistic Relay Selection (SR-ORS) Method for a Dual-hop Multiple Full-duplex Bi-directional Wireless Relaying Networks,” Proc. Of the 2016 National Conf. on Electrical, Electronics and Biomedical Engineering (ELECO), pp. 437-441, 2016.
[37] A. Goldsmith, Wireless Communications, ISBN-13: 978-0-521-83716-3, Cambridge University Press, 2005.
[38] T. S. Rappaport, Wireless Communications: Principles and Practice, 2nd Edn., Prentice Hall, 2002.
[39] V. Ozduran, “LDPCC and OFDM Based Cooperative Communication for Wireless Sensor Networks,” Balkan J. of Electrical and Computer Engineering, vol. 8, no. 3, pp. 201-208, DOI: 10.17694/bajece.688294, 2020.

[40] V. Ozduran, "Sum-rate Based Hybrid Half/Full-duplex Relay Selection in a Dual-hop Two-way Wireless Relaying Networks," Proc. Of the 2017 IEEE Int. Conf. on Sensing, Communication and Networking Workshops (SECON Workshops), pp. 1-5, DOI: 10.1109/SECONW.2017.8314983, 2017.

[41] V. Ozduran, E. Soleimani-Nasab and B. S. Yarman, "Sum-rate Based Relay Selection with Feedback Delay for a Multiple Half/Full-duplex Two-way Relaying," Proc. Of the 2017 15th Int. Conf. on ITS Telecommunications (ITST), pp. 1-7, DOI: 10.1109/ITST.2017.7972196, 2017.

[42] V. Ozduran et al., "Sum-rate Based Opportunistic Relay Selection with Channel Estimation Error for a Dual-hop Multiple Half/Full-duplex Bi-directional Wireless Relaying Networks," Proc. Of the 2017 26th Wireless and Optical Communication Conf. (WOCC), pp. 1-6, DOI: 10.1109/WOCC.2017.7929009, 2017.

[43] V. Ozduran, B. S. Yarman and J. M. Cioffi, "Feedback Delay Effects on Physical Layer Security in a Dual-hop Half/Full-duplex Bi-directional Wireless Relaying Networks," Proc. Of the 2016 IEEE Globecom Workshops (GC Wkshps), pp. 1-7, DOI: 10.1109/GLOCOMW.2016.7848907, 2016.

[44] N. V. Toan, N. N. Lan, T. T. Duy, P. N. Son and N. T. Hieu, "Fountain Codes-based Hybrid Satellite-terrestrial Relay Multicast Schemes in Co-channel Interference Environment: Outage Performance, Joint Time and Power Allocations," Jordanian Journal of Computers and Information Technology (JJCIT), vol. 12, no. 2, pp. 166-182, DOI: 10.5455/jjcit.71-1769912165, 2026.

ملخص البحث:

تبحث هذه الورقة في أداء شبكة ترحيل ثنائي الاتّجاه مخصّصة لشبكات الاستشعار اللّاسلكية، تجمع بين تقنيتي ترميز "النّافورة" وترميز الشبكة الرّقمي في ظلّ وجود تداخل في القناة المشتركة. تمّ النّظر في بروتوكول إرسال مكوّن من ثلاثِ مراحل ومقارنته بالبروتوكول التّقليدي المكوّن من أربعِ مراحل ويستخدم ترميز النّافورة. ولعزل مساهمة ترميز النّافورة، تمّ تقديم نموذجٍ مرجعي إضافي يعتمد على ثلاث مراحل دون ترميز (مع تكرار ثابت) وبالميزانيةِ نفسها، حيث يتمّ توزيع فُرص الإرسال (Q) على (H) من الحزم غير المرمّزة والمتميزة.

وفي ظلّ ظروف تلاشي الإشارة المستقلّ بنمط "بلوك-رايلي"، تمّ اشتقاق تعبيراتٍ تحليلية بصيغةٍ مغلقة لاحتمالات انقطاع الخدمة عند العقدتيْن الطّرفيتيْن، مع أخذ التّداخُل في القناة المشتركة عند كل من عُقدةِ التّرحيل وعُقدة المصدر بعين الاعتبار. وتظهر عمليات محاكاة "مونت كارلو" التي اعتمدت على مليون حالة للقناة تمّ توليدها بشكلٍ مستقلّ لكلّ نقطة بيانية، توافقاً وثيقاً مع التّعبيرات التّحليلية المشتّتة.

وتبيّن النّتائج العدّدية أنّ المخطّط المقترح يحقّق احتمالات انقطاعٍ أقلّ ومجموع إنتاجية ثنائي الاتّجاه أعلى مقارنة بالنّماذج المرجعية. علاوة علىً ذلك، تُظهر المقارنة أنّ احتمالات الانقطاع تستمر في الانخفاض عند غياب التّداخل أو عند بقاء قدرته ثابتة، في حين أنّ التحجيم النّسبي لقدرة الإشارة المطلوبة مقابل قدرة التّداخل يؤدّي إلى ظهور مستوياتٍ دنيا لاحتمالية الانقطاع بقيمٍ غير صفرية.